PROGRESS REPORT SUMMARY	GRANT NUMBER HL70262-08	
	PERIOD COVERED BY THIS REPORT	
PRINCIPAL INVESTIGATOR OR PROGRAM DIRECTOR Ajit P. Yoganathan	FROM 05/16/11	THROUGH 06/30/13

APPLICANT ORGANIZATION

Georgia Tech Research Corp.

TITLE OF PROJECT (Repeat title shown in Item 1 on first page)

Computational Modeling of Mechanical Heart Valves

A. Human Subjects (Complete Item 6 on the Face Page)
Involvement of Human Subjects ☒ No Change Since Previous Submission ☐ Change

B. Vertebrate Animals (Complete Item 7 on the Face Page)
Use of Vertebrate Animals ☒ No Change Since Previous Submission ☐ Change

SEE PHS 2590 INSTRUCTIONS.

WOMEN AND MINORITY INCLUSION: See PHS 398 Instructions. Use Inclusion Enrollment Report Format Page and, if necessary, Targeted/Planned Enrollment Format Page.

a. Specific Aims

There are no changes to the original specific aims.

b. Studies and Results

OVERALL SUMMARY

The overall progress of the grant during the last 5 years is described below. We have integrated and tested several high-resolution experimental and computational methods to develop a translational research platform for the verification and validation of medical imaging-based computational models. These models are aimed to provide predictive assessment of the performance of cardiac devices post-implantation (including but not limited to prosthetic heart valves) prior to *in vivo* intervention. For the first time, we have validated a computational fluid-structure interaction (FSI) solver specifically developed to simulate internal flow induced by moving boundaries as seen in the human left ventricle (LV). Two types of experimental *in vitro* test beds have been developed and tested for this purpose: a tetrahedral chamber with a single moving wall and an anatomical flexible-walled LV physical model. Multiple modalities of state-of-the-art experimental diagnostics, including high-speed stereo photogrammetry, particle image velocimetry (PIV) and cardiac magnetic resonance imaging (MRI) have been used to obtain high spatiotemporal resolution data of the wall motion kinematics and flow fields to use for validating FSI simulations. In addition, a separate computational method has been developed that can model pulsatile flows through prosthetic cardiovascular devices with the presence of realistic platelets. This method employs optimal parallel processing with very high spatiotemporal simulations to quantify blood damage in cardiovascular flows. This generic method can also be used for a variety of other flow conditions and medical devices as well.

We have developed advanced image processing methods to reconstruct the *in vivo* wall motion and flow fields. We have validated the accuracies of these methods using our *in vitro* experimental platforms using benchmark data obtained using higher spatiotemporal experimental modalities. Finally, several sub-studies examining the interaction between anatomical components of the LV, including the mitral annulus and mitral leaflet length, on filling fluid dynamics have been investigated. We have also conducted detailed studies on the effect of varying heart rate on diastolic flow patterns to investigate the impact of mild and moderate exercise. These fundamental studies conducted under controlled conditions *in vitro* and *in silico* provide a previously unavailable physical insight into the fluid flow experienced within the LV under normal and altered functional conditions. The results of these studies can be used to optimize the design of cardiac devices such as prosthetic heart valves and mitral annuloplasty rings. Future directions of this work involve optimizing well known current designs, but also evaluating newer devices such as percutaneous valves. This can be performed as a pre-clinical assessment of novel devices. In the long-term, we intend to further our clinical translational framework to employ computational modeling for patient specific geometries for use in

surgical planning and intervention.

SPECIFIC AIM I: Development of CFD tools for left ventricle/aorta configuration

1. The Development of an efficient solver for left heart hemodynamics simulations

The left heart system is a complex system consisting of several organs. Each organ has its own physiological functionality and constraints. The left heart system is depicted in Figure 1. It consists of two main parts: i) the left ventricle (LV) and ii) the aorta. We simplify the system by assuming that the atrium and the descending aorta are truncated from the whole cardiovascular systems. Appropriate boundary conditions are applied in the domain interface. For example, the inlet and outlet boundaries are specified using measured quantities. The motion of the left ventricle can be obtained via non-invasive measurements of patients or results of cell-based activation models.

In order to model this complex system, we develop an overset-curvilinear immersed boundary (overset-CURVIB) method in general non-inertial frames of reference to deal with this situation. Our numerical method incorporates overset-curvilinear grids to efficiently handle multi-connected geometries and increase the resolution locally near the immersed boundaries. Complex bodies undergoing arbitrarily large deformation may be embedded within the overset-curvilinear background grid and treated as sharp interfaces using the curvilinear immersed boundary (CURVIB- (Ge and Sotiropoulos, 2007)). The blood flow (incompressible fluid) equations are formulated in a general non-inertial frame of reference to enhance the overall versatility and efficiency of the numerical approach. Efficient search algorithms to identify areas requiring blanking donor cells and interpolation coefficients for constructing the boundary conditions at grid interfaces of the overset grid are developed and implemented using efficient parallel computing communication strategies to transfer information among sub-domains. The governing equations are discretized using a second order accurate finite-volume approach and integrated in time via an efficient fractional step method. Various strategies for ensuring globally conservative interpolation at grid interfaces suitable for incompressible flow fractional step methods are implemented and evaluated. The method is verified and validated against experimental data and its capabilities are demonstrated by simulating the systolic phase in an anatomic left ventricle with an implanted mechanical heart valve in the aortic position as the final check.

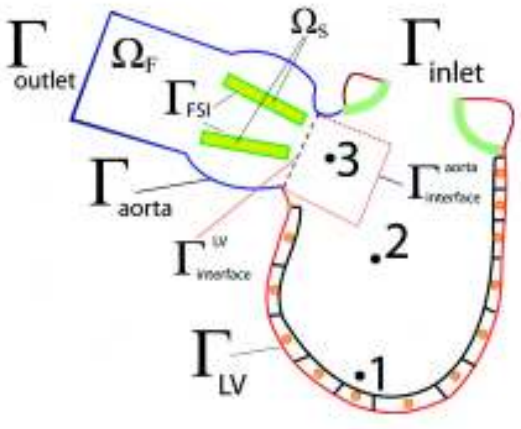

Figure 1. The sketch depicts the computational framework and the partition between the fluid and the solid domains. Γ_{inlet} and Γ_{outlet} are the inlet and outlet of the computational domain. Γ_{aorta} is the aortic portion of the domain where the no-slip boundary condition is applied. Γ_{FSI} is the interface between leaflets Ω_s and the blood flow Ω_F, which is simulated via the fluid-structure interaction methodology. The Γ_{LV} represents the endocardium surface where the left ventricle beats. The kinematics of Γ_{LV} can be obtained via non-invasive measurement in patient or simulation results of the cell-based model.

2. Kinematic models for patient-specific left ventricle

In order to simulate the motion of the left ventricle, we reconstruct the anatomic left heart geometry from MRI data of a healthy subject. The aortic and mitral valve, coronary and carotid arteries as well as one part of the left atrium are removed from the original anatomy. The final geometry is shown in Figure 2. The values for the

various geometrical parameters of our LV model are as follows: the LV long and short axes lengths are L=80 mm and D_L=47 mm, respectively; the mitral annulus diameter is D_M=37 mm;

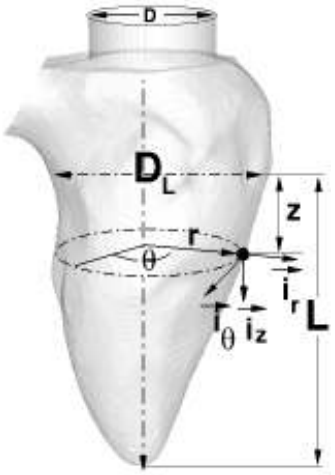

Figure 2. The left heart model reconstructed from MRI images. (r,θ, z) is the cylindrical coordinate system defined for the LV with corresponding unit vectors i_r, i_r , i_z. L and D_L are the lengths of the long and short LV axes, respectively.

To model the LV kinematics we use the cell-based electric excitation methodology. The approach follows lumped-type parameter models (Beyar and Sideman, 1986; Beyar and Sideman, 1984,; Chadwick, 1982), which, nevertheless, is able to reproduce the physiological features of the LV kinematics. The model is based on the following assumptions: 1) Only the LV moves. The atrium and the LV base remain stationary in the cardiac cycle; 2) Only the endocardium is modeled as the wall surface. The endocardium surface is discretized with an unstructured grid with material nodes as shown in Figure 3. Each material node is assumed to represent one endocardium cell; and 3) The response of the endocardium cell to the cardiac electrical stimulation is assumed to be a function of a time-dependent potential p (t).

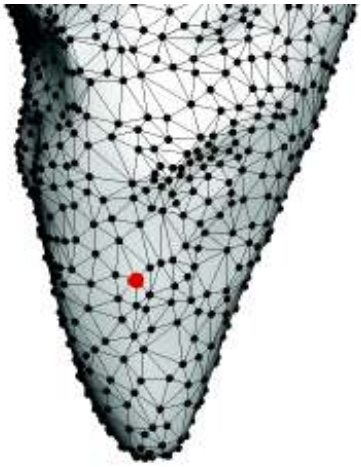

Figure 3. The moving LV model, discretized with the unstructured grid is immersed in a background stationary curvilinear mesh as required by the CURVIB method. The blood flow is driven by the LV wall motion resulting from the cell-activation model. The "red" material point denotes one material point on the LV surface.

To demonstrate that the emerging, large-scale LV wall kinematics resulting from the proposed model is physiologic, major global LV kinematics parameters calculated from the model are compared with available *in vivo* data. The most important parameter during diastole is the E-wave velocity at the mitral orifice. In our case, the E-wave peak velocity, which is estimated as the bulk velocity from the mitral inflow wave from,

reaches 70 cm/s. This value is in the range of measurements obtained from *in vivo* MRI, which range from 50 to 70 cm/s (Saber et al., 2001; Schenkel et al., 2009b) .

The instantaneous direction of the calculated wall velocity field is visualized in Figure 4 in terms of instantaneous LV wall streamlines at several instants during the cardiac cycle. The cell-activation model produces wall surface motion that exhibits complex twisting motion as it relaxes in the clockwise direction (looking from the base) during diastole and contracts in the counter-clockwise direction during systole. These twisting patterns are consistent with *in vivo* observations (Hunter et al., 2003,), in which the rotation of the apex relative to the base is in the counter-clockwise direction during systole and clockwise during diastolic untwist (as viewed from the base).

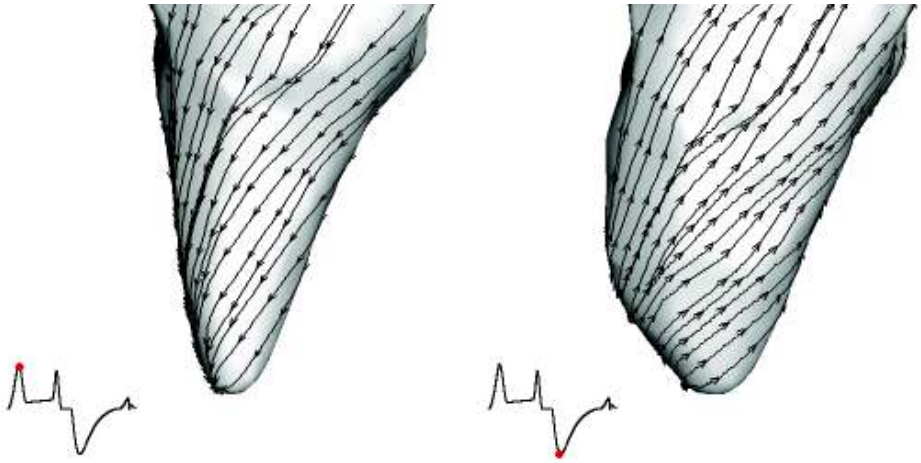

Figure 4. The deformation of the endocardium surface during one cardiac cycle from diastole to systole. The instantaneous wall velocity field is indicated by the projected streamlines on the endocardium surface. The red dot in the inset shows the time instance in the cardiac cycle.

The calculated LV volume rate of change dV/dt during one cardiac cycle is shown in Figure 5. During diastole, the distinct early diastolic filling peak (E-wave) is separated from the passive filling peak (A-wave) by a phase of very slow volume expansion, referred to as diastasis. An important physiologic parameter is the ratio of the E- and A-waves dV/dt, peaks (E/A ratio). As shown in Figure 5, the E/A ratio resulting from our model is approximately 1.1, which is in good agreement with physiologic values (Kim et al., 1995; Thomas and AE, 1991). In the systolic phase, the dV/dt resulting from the model becomes as low as -19 liter/min is also well within the physiologic in the order of -20 liter/min (Yoganathan et al., 2004). The details of the derivation have been published in the Journal of Computational Physics (Le and Sotiropoulos, 2012a).

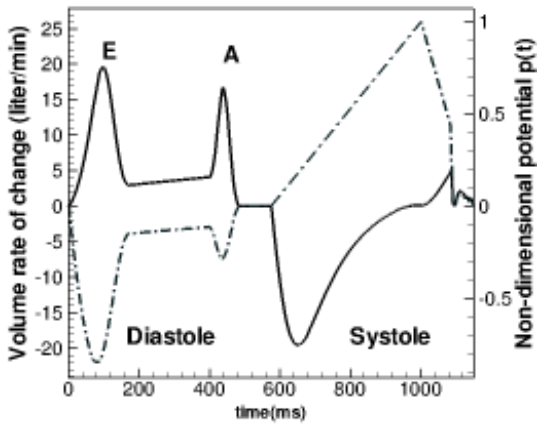

Figure 5. The left ventricle volume rate of change during one cardiac cycle. There are two distinct positive E-wave and A-wave peaks separated by the diastasis during diastole. The negative peak is the systolic peak.

3. Simulations of Pulsatile BMHV Suspension Flow using Parallelized LBM-EBF Method:

An alternative numerical method is employed to study platelet damage in BMHV flows. These computational studies employ a lattice Boltzmann with external boundary force (LBM-EBF) method for platelet flow simulations. In this method, the fluid flow is solved using the lattice Boltzmann method, and each platelet is mapped onto a Lagrangian frame moving through the fluid domain. Platelets are realistically shaped as ellipsoidal particles, and not as point particles as in other limited computational studies. The two-way fluid-solid interactions are enforced with no-slip conditions by the external boundary force method. The motion and orientation of the platelet are obtained from Newtonian dynamics equations. The use of the lattice Boltzmann method for particle suspension fluid flows has been extensively validated. The LBM-EBF FSI solver has the ability to track the interaction forces (collisions and shear) of platelets flowing through BMHVs and can thus be used to evaluate blood damage. The advantages of this method are in its parallel computation (shown to scale to 96.6% of ideal efficiency at 16,384 computational cores), multiscaling (modeling particles with subgrid resolution), and realistic particle modeling (platelets with mass and volume and meshed surfaces).

The first two studies using LBM-EBF have been published (Wu *et al.* 2011, Yun *et al.* 2012), where the platelet damage quantification method was validated. This was performed against experimental blood damage results and for flows through actual BMHV hinges. These papers have validated the numerical method for modeling platelet damage, particularly for BMHV flows.

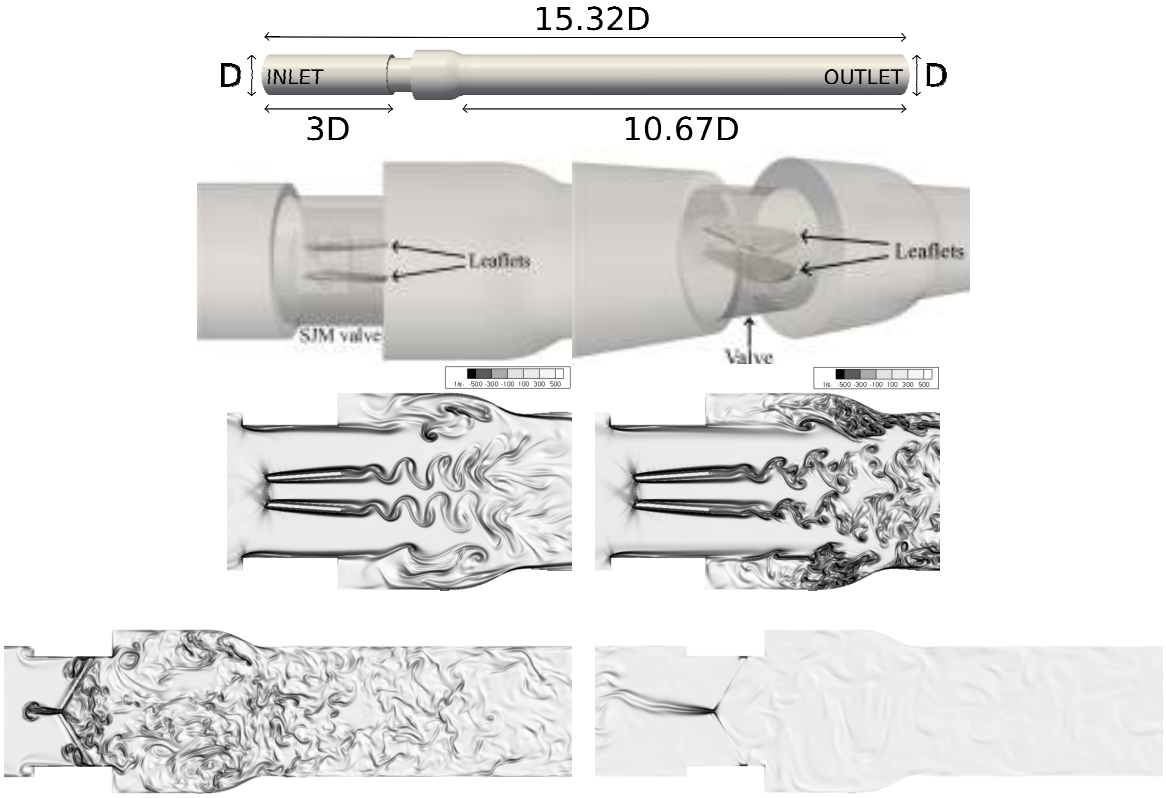

Figure 6. A) The computational model of the experimental setup, B) Side and angled transparent views of the SJM valve, C) 5 time points from acceleration to peak systole to valve closure and diastole for pulsatile BMHV flow.

The LBM fluid solver has been validated by simulating single-phase fluid pulsatile flow through a SJM regent valve for an entire cardiac cycle and comparing the results with experiments of pulsatile flow of a blood analog fluid through a SJM valve in an *in vitro* loop with the same design (same geometry, leaflet motion, boundary conditions and blood kinematic viscosity). The instantaneous time snapshots of out-of-plane vorticity in the perpendicular plane are shown in 2D snapshots (Figure 6) with the highest spatiotemporal resolution to date (80μm, 2.4μs). This includes reverse flow and the ability to capture the smallest scale eddies in this complex, high Reynolds number flow. Particularly evident are vortex shedding past the leaflet tips and past the sinus expansion step. Once the leaflets close, leakage jets are formed in the central orifice and through the leaflet-valve gaps. These results were all obtained after simulation of two full cardiac cycles

to remove the effect of initialization to peak flow.

Figure 7. 5400 platelets throughout BMHV after end of systolic flow modeling, with leaflet closure.

Simulations are then modeled with platelets released during pulsatile flow through the BMHV. 5400 platelets are released, with 300 platelets released every 20ms during the systolic flow phase (Figure 7). Platelets are released upstream of the valve at the same axial position but with random cross-sectional positions and orientations. Highest damaged platelets are found residing in the valve and sinus regions, despite 64% of platelets advecting downstream of the sinus at the simulation end timepoint. The highest damaged platelets are found near the leaflet surfaces, valve walls, and near the walls of the sinus expansion.

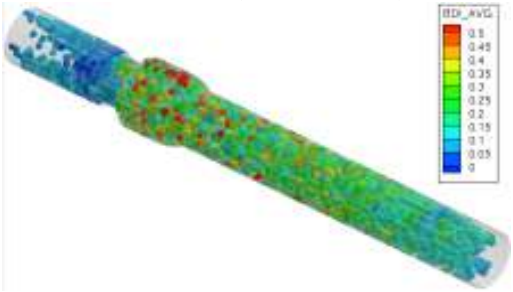

Figure 8. Contour plot of platelet BDI (dynes s/cm^2) – Eulerian view

For Eulerian views (figure 8), the flow domain can be partitioned into small regions, and average damage in each region can be determined. From this, a platelet damage contour plot is created showing the evolution of platelet damage in space, over time. The largest number of high damage regions is found in the sinus expansion near the walls. The flow in the sinus expansion is characterized by strong vortices and recirculation regions. This is particularly dangerous as increased platelet residence time in the recirculation region could lead to platelet activation, consistent with previous results based on a model geometry.

For a Lagrangian view (Figure 9), platelets with highest accumulated damage are isolated and pathlines are mapped. This can be viewed in multiple angles and connected with flow fields, showing how instantaneous platelet damage and instantaneous flow features are connected. This can also be used as a guideline for future single-phase flow simulations to interpret flow results and connect results with potential for blood damage complications.

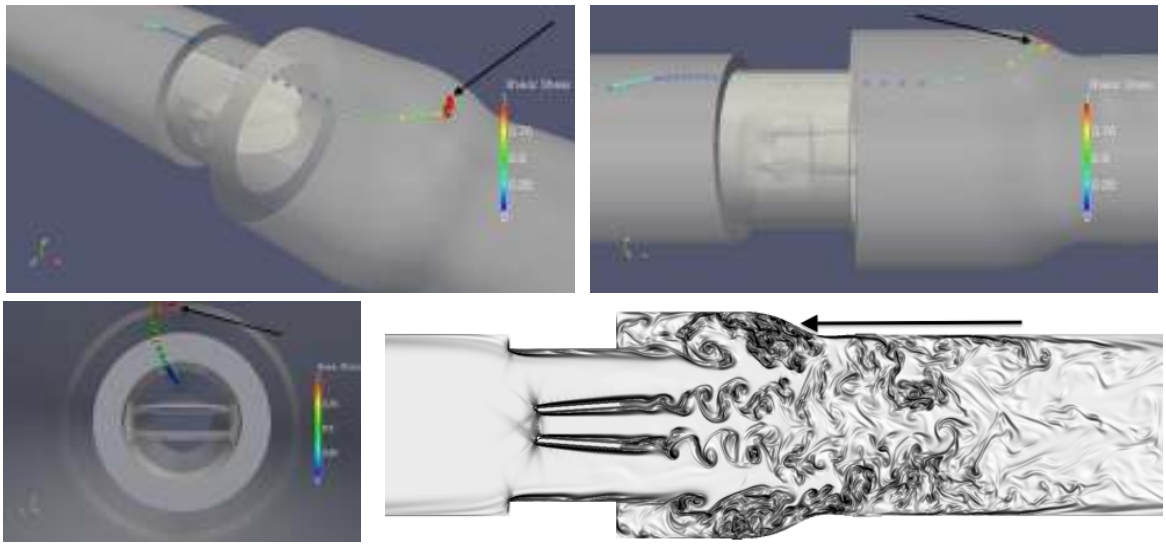

Figure 9. Particle tracking showing highlighted platelet damage path and associated flow field

This baseline case is performed for a SJM valve with physiologic adult conditions, and has demonstrated the capabilities of LBM-EBF as a numerical tool to evaluate the blood damage performance of medical devices. BMHVs are a suitable initial case due to the simplified geometry and flow, and the extensive

previous data available for comparison. The numerical method can be applied to model various cardiovascular flows and devices. This can be applied to pediatric applications for BMHVs, to be used as a predictive assessment of the fluid mechanics performance and blood damage performance of pediatric sized BMHVs. This is also useful for new devices that have not undergone significant analysis. For example, percutaneous valves or left ventricular assist devices require accurate assessment of both generic device performance and blood damage performance, which can be provided by the numerical method.

SPECIFIC AIM II: In vitro experiments for validation in a phantom left ventricle/aorta configuration with moving boundaries

1. Pulsatile Flow Loop:

One of the Georgia Tech Left Heart Simulators used for the experimental validation is shown in Figure 10. The model left ventricle is an acrylic truncated tetrahedron with a single flexible wall made of latex. The motion of the flexible membrane is driven by a Vivtro Superpump System pump (Model SPS3891, Vivitro Systems; British Columbia). There is a 23mm St. Jude Medical Regent BMHV is housed just below the aortic sinus in the simulator. Downstream of the aortic section (red) there is an ultrasonic flow probe (Model ME-PXN, Transonic Sonic Systems; Ithaca, NY). The compliance chamber and point resistance are used to control the hemodynamic waveforms. The mitral inflow comes from the reservoir and through another ultrasonic flow probe, and no mitral valve is positioned at the mitral orifice at this stage. Directionality of the flow was maintained using a unidirectional valve 15 diameters upstream of the mitral orifice. Flow conditioners are included 10 valve diameters upstream of the mitral orifice and are used to reduce the influence of the non-streamwise components to obtain a uniform velocity field as the inflow to the ventricle.

2D digital particle image velocimetry measurements can be performed at the mitral inflow tract, ventricle, and the flow through the BMHV in the aortic section. 50 phase locked measurements are ensemble averaged to construct velocity fields in each region. Stereo-photogrammetry is used to track the kinematics of the flexible membrane. The hemodynamic data acquisition system consists of two flow probes Q1 and Q2 (Model ME-PXN, Transonic Sonic Systems; Ithaca, NY) and three pressure transducers (TruWave Disposable Pressure Transducers, Edwards Lifesciences; Irvine, CA). The inline flow probes are used to measure the instantaneous flow upstream of the mitral orifice to the ventricle and the downstream flow through the aorta. The instantaneous absolute pressure measurements are measured upstream of the mitral valve, downstream of the aortic valve, and near the apex of the ventricle as shown in Figure 6. A trigger signal activates the acquisition of the flow field measurements using 2D digital particle image velocimetry (DPIV), flexible membrane position tracking using high-speed stereo photogrammetry, and the instantaneous hemodynamic variables. The trigger is an analog pulse created in LabView and output by a National Instruments DAQ system. The DAQ output waveform to the piston can be modified to change the contraction/relaxation timings and flow magnitude to simulate disease. The changes to the kinematic of flexible membrane and the fluid mechanics within the system can be recorded.

The model described above has since been redesigned and improved both structurally and functionally. The new Georgia Tech Left Heart Simulator is shown in Figure 11. The left ventricular geometry was generated in Solidworks™ (Dassault Systèmes Solidworks Corporation**,** Waltham, MA, USA) by constructing a series of concentric elliptical sketches on parallel planes connected by spline curves. A 125° cut was made at the base of the ventricle such that the mitral and aortic annular planes matched *in vivo* conditions. The ventricle is encased in an acrylic chamber to which a pulsatile linear actuator is connected. The linear actuator causes a change in pressure in the outer chamber, which in turn forces the ventricle to contract and relax. The system is then placed in a similar flow loop as the simplified model (Figure 12). Pressure measurements can also be taken at the atrium, ventricle, and aorta. Flow measurements are taken at the inflow and outflow of the ventricle.

The advantage of this simulator is in its MRI and echocardiography compatibility, which provides a direct link between bench top and clinical modalities. This allows for a comparison between planar flow fields from PCMR and PIV, wall motion from stereo-photogrammetry and CMR, mitral and aortic flow rates from PCMR and flow probes, etc.

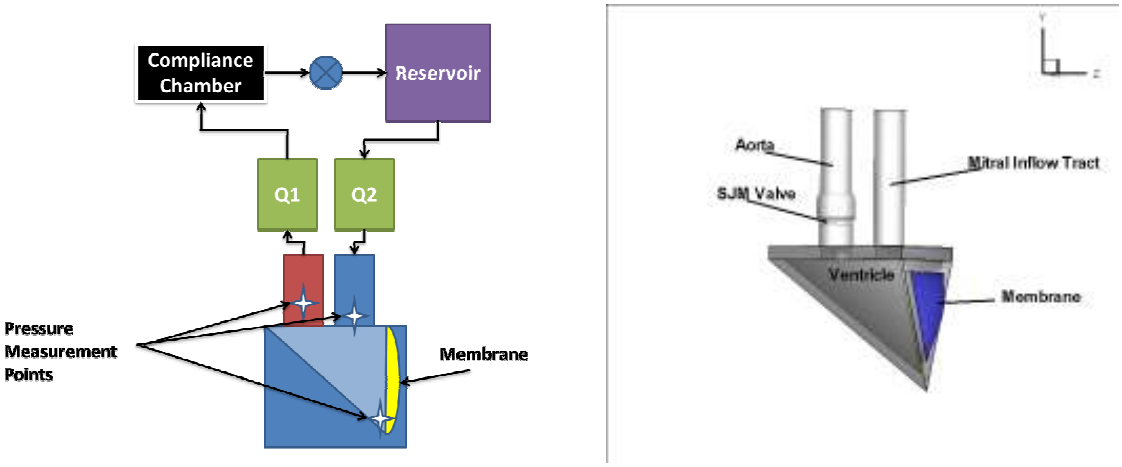

Figure 10. Left: The simplified model of a left ventricle with mitral inlet (blue) and the aortic outlet (red). The BMHV is implanted at the aortic position just below the aortic sinus. Right: schematic of the ventricular chamber with membrane (blue), inflow and out flow tracts.

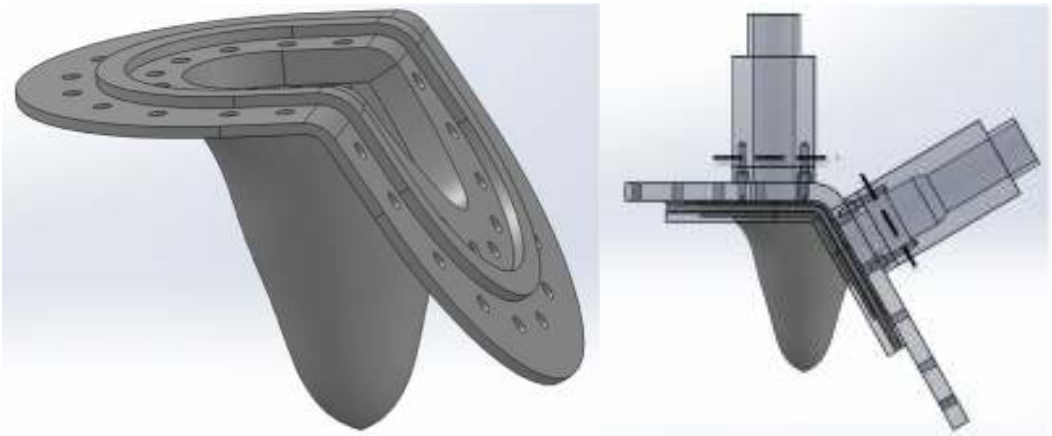

Figure 11. Left: The realistic model of a left ventricle with mitral inlet and the aortic outlet. BMHVs are implanted at the mitral annulus and aortic annulus just below the aortic sinus. Right: schematic of the realistic ventricular bag membrane.

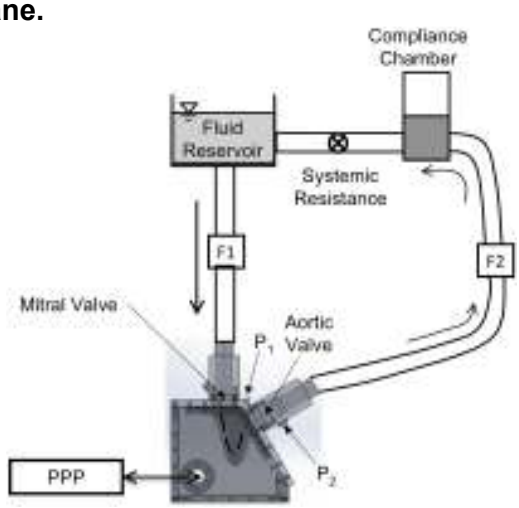

Figure 12. Schematic of new flow loop for the realistic Georgia Tech Left Heart Simulator.

For the validation of FSI models of the left heart complex, three sets of experiments were conducted on phantom left ventricle models. The design of each experiment was selected to gradually include more complexity in the system. The first set of experiments used the idealized left ventricle model consisting of a tetrahedral chamber. The fluid dynamics of diastolic filling through inclined inflow nozzles, coarsely representing the asymmetry of mitral leaflets, was investigated as a part of this sub-study. Numerical simulations for this setup were conducted in tandem and the flow field results were compared to experiments for validation. The second and third sets of experiments were conducted on the anatomical left ventricle model, to examine the effects of varying the mitral annulus shape (between D- and O-orifices) and heart rate (100 bpm and 120 bpm).

2. Validation of vortex formation phenomenon in complex geometries

2.1 Vortex ring formation from inclined nozzles

In order to validate our computational framework to simulate complex flows in the left ventricle, we validate our numerical procedures with well-controlled experimental data. The first validation is the investigation of vortex dynamics in laminar, impulsively driven flows through inclined nozzles in a piston-cylinder apparatus. Our simulations are motivated by the need to provide a complete description of the intricate vortical structures and governing mechanisms emerging in such flows as documented in the experiments of (Troolin and Longmire, 2010). Our computational result agrees well with the experimental data as shown in Figure .

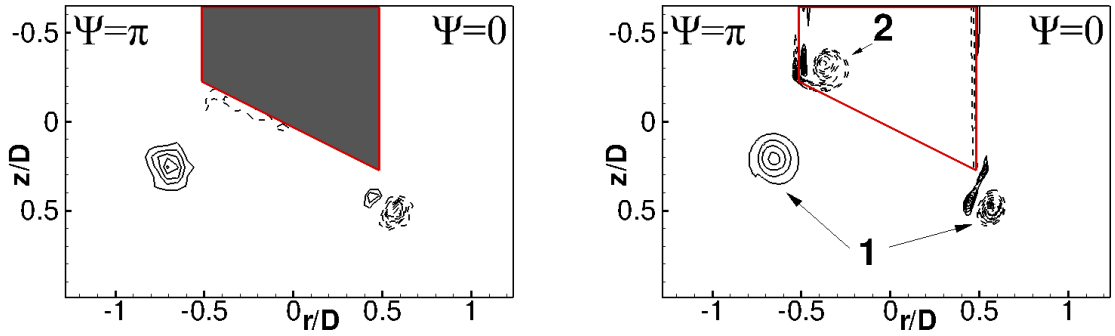

Figure 13. Comparison between a) measured (Webster and Longmire) (left) and b) computed (right) instantaneous non-dimensional, out-of-plane vorticity contours for the inclined nozzle on the symmetry plane. The first contour is 5 U/D and the increment is 2.5 U/D. Dash lines indicate negative vorticity values. Ring 1 and 2 are the primary and secondary (stopping) rings.

We show that the flow is dominated by the interaction of two main vortical structures: the primary inclined vortex ring at the nozzle exit and the secondary stopping ring that arises due to the entrainment of the flow into the cylinder when the piston stops moving. These two structures are connected together with pairs of vortex tubes, which evolve from the continuous vortex sheet initially connecting the primary vortex ring with the interior cylinder wall as seen in Figure . In the exterior of the nozzle the key mechanism responsible for the breakup of the vortical structure is the interaction of the stronger inclined primary ring with the weaker stopping ring near the longest lip of the nozzle. In the interior of the nozzle the dynamics are governed by the axial stretching of the secondary ring and the ultimate impingement of this ring on the cylinder wall. Our simulations also clarify the kinematics of the azimuthal flow along the core of the primary vortex ring. We show that the azimuthal flow is characterized by a pair of two spiral saddle foci at the long and short lips of the nozzle through which ambient flow enters and exits the primary vortex core. The details of the comparison and computational results can be found in the Journal of Fluid Mechanics (Le et al., 2011).

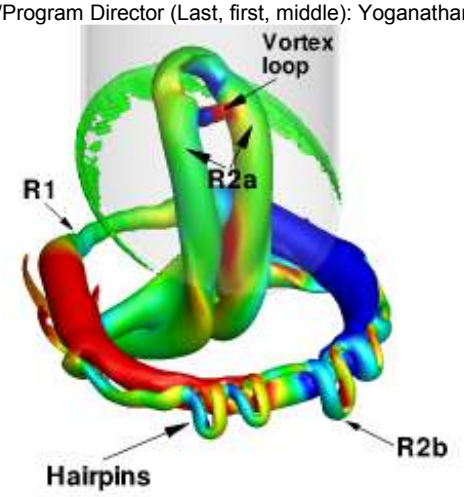

Figure 14. The three-dimensional topology and evolution of the vortical structure for the inclined nozzle visualized by plotting the iso-surface of non-dimensional vorticity magnitude colored with contours of non-dimensional helicity density. The vorticity dynamics during this early stage is characterized by the formation and interaction of the primary ring (R1) and the stopping ring.

2.2 Vortex ring formation in idealized left ventricle models

In order to examine the vortex formation process of the left ventricle in a well-controlled condition, we carry out an experiment with an idealized model of the LV. The idealized LV consists of a tetrahedral chamber representing the LV. The mitral and aortic orifices are connected to a circular pipe as shown in Figure . Particle Imaging Velocimetry (PIV) measurements are carried out on representative planes to provide sufficient data in order to validate the numerical model.

The computational model closely follows the experimental setup. The diameter of the mitral orifice is D = 1 inch (25.4 mm). The viscosity of the working fluid is set as the experimental value of 3.5×10^{-6} m^2/s. The inflow waveform at the mitral orifice is shown in Figure with the peak flow rate of Q = 16 L/min and the bulk velocity corresponds to this flux is U = 0.52 m/s.. The peak Reynolds number is therefore Re = UD/u= 3943. A structured grid with size of 45 million grid points is used to simulate this case. The computational grid is a box covering the size of the LV chamber. The aortic outlet is specified using homogeneous Neumann boundary condition (no resistance).

The simulation results are compared with the experimental data on the measured plane shown in Figure . Good agreement between the experiment and numerical simulation are shown at early diastolic filling as seen in Figure at t=300 ms. All important features of the flow are captured accurately by the computational model. The main structure is an asymmetrical vortex ring, which is indicated by the negative and positive vorticity cores as shown in Figure . At early diastole, this vortex ring is formed at the mitral orifice tip and propagates toward the apex of the LV chamber. Note that due to the asymmetrical configuration of the geometry, the vortex core near the aortic orifice (negative) grows significantly faster than the other. The negative core also impacts directly with the LV solid wall right after formation. The computational model also simulates correctly the vorticity extraction created by the impingement of this vortex ring on the inclined wall surface. The three-dimensional structure of this vortex ring is shown in Figure . The vortex core thickness varies continuously along the ring's circumference indicating a deviation from the perfectly circular ring.

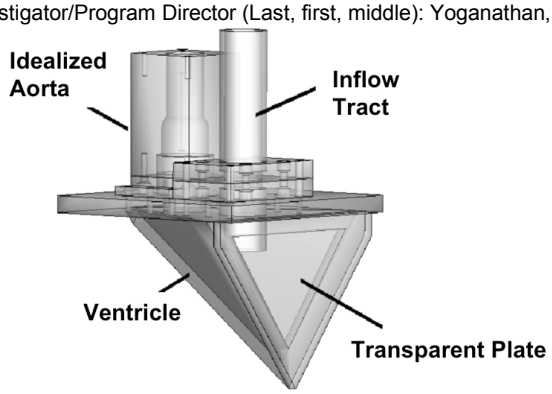

Figure 15. The schematic of the idealized left ventricle (tetrahedral chamber) and the corresponding components

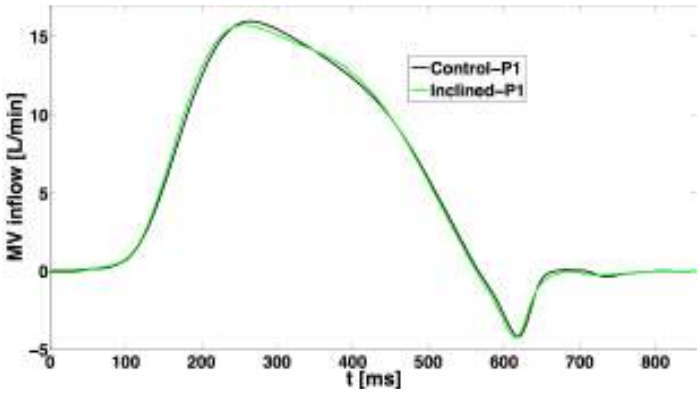

Figure 16. The volume flow rate at the mitral orifice during one cycle

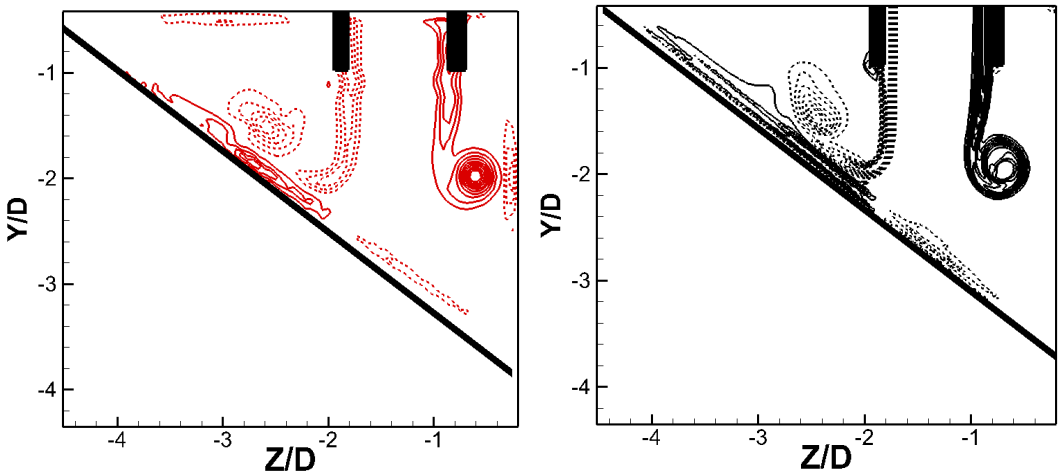

Figure 17. Comparison between measured (PIV - left) and computed (CFD - right) results at t=300ms on the symmetry plane of mitral orifice. The flow is visualized by out-of-plane vorticity contour. The dash line indicates the negative values. All values are non-dimensionalized by the mitral orifice diameter D and the velocity scale U

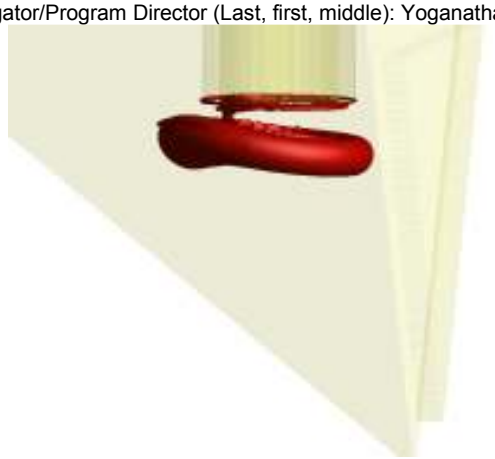

Figure 18. Formation of the vortex ring inside the idealized left ventricle at t = 260 ms. The vertical structure is visualized using Q-criteria(Hunt et al., 1988).

3. Effect of Mitral Annular Shape on Ventricular Filling Fluid Dynamics

The natural geometry of the mitral annulus is D-shaped; however, after BMHV implantation, the annulus is forced to take on the geometry of the valve housing (O-shape). The goal of this study was to explore the effect of geometrical modification on intra-ventricular filling dynamics. In addition, mitral annular geometry during diastolic filling takes on a circular shape. However, all current designs of mitral annuloplasty rings use a D-shaped orifice geometry . To isolate effects of annulus geometry, the leaflets of the valves were not included in this study. Figure 19 (a) and (b) show geometrical designs of the mitral annulus used in this study. Particle image velocimetry was used to quantify the differences between the flow fields of the two annulus shapes. As shown in Figure 20 the diameter of the incoming jet during peak diastole for the D-shaped orifice is significantly smaller than that of the O-orifice. More importantly, however, there is more shearing on the clockwise rotating vortex ring formed close to the lateral wall. This is can be seen comparing Figure 20. Also, the strength of the vortex rings formed is much lower in the D-annulus compared to the O annulus.

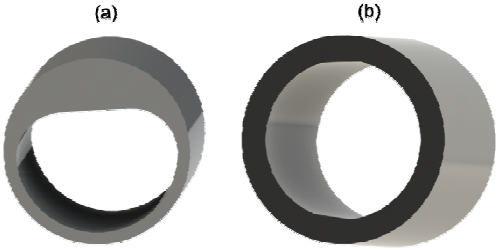

Figure 19. (a) D-shaped mitral annulus. (b) O-shaped mitral annulus.

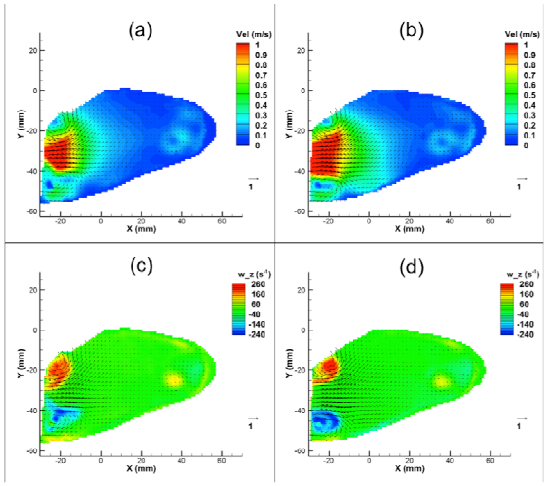

Figure 20. Velocity (top) and vorticity (bottom) plots at peak diastole comparing O (right) and D (left) shaped annulus.

4. Effect of Heart Rate on Ventricular Filling Fluid Dynamics

Computational fluid-structure interaction (FSI) models of the left heart employing medical imaging data as input conditions need to be validated rigorously against a wide range of system parameters, including heart rate, stroke volume, aortic pressure and LV inflow patterns, to name a few. Varying heart rate increases the velocity of ventricular wall motion, which inevitably presents a challenge for FSI solvers specific to the temporal resolution needed to accurately predict the resultant intra-ventricular flow field. In this experimental sub-study, we varied the heart rate in our physical model of the LV to examine intra-ventricular flow fields during diastolic filling, under mild and moderate exercise conditions of 100 bpm and 120 bpm, respectively. The results of the study were compared to the baseline heart rate case of 70 bpm presented in the previous sub-section. All the heart rate studies employed a D-shaped mitral annulus without including mitral valve leaflets, so as to decouple the role of the leaflets on the resultant flow. The ventricular inflow E/A ratio ranged between 1-1.1 across all three heart rates. All the other experimental conditions, including LV pressure, aortic pressure and stroke volume, were maintained constant across all three heart rates. 2D PIV was used to visualize the intra-ventricular flow field across multiple time instants in the diastolic phase of the cardiac cycle. The results of the study show that with increasing heart rate, the circulation strength of the inflow vortex ring (as indicated by the area of the core) formed during peak diastolic filling decreases. This is related to the amount of actual time available for the active suction phase (E-wave) of the LV wall motion during when the intra-ventricular pressure gradient is negative. In addition, the propagation of the vortex ring is strengthened in the atrial kick portion of the diastolic phase under conditions of moderate exercise of 120 bpm. These results suggest that though the vortex ring formation during exercise is initially limited by the short time available for the E-wave, the importance of the atrial kick in propagation and further entrainment is elevated.

SPECIFIC AIM III: Develop image processing methods for reconstruction of anatomically accurate moving ventricle and aorta geometries

1. MR Imaging

MRI scans have been performed to complete the volunteer study. We have also coordinated with Emory Healthcare for the patient study. The acquisition protocol has not changed, but we performed a different type of temporal scan that would alleviate the patient from having to hold their breath 15 times (1 per slice) when scanned, and would have eliminated breath-hold shifts. The scanning protocol was modeled after the Whole Heart protocol, but applied to 18 time points in the cardiac cycle. The scan took approximately and hour and half. The use of this type of acquisition sequence for the patients could have made the experience less stressful for the patient, but there was increased blurring of the images throughout systole and would make segmentation of the geometry difficult.

2. Segmentation of time-resolved MRI images

The cine-MRI images acquired in the course of this grant contains information on the motion of the scanned region, that need to be accurately extracted to design a moving geometrical model of left ventricle and aorta. The first step in this process is the “segmentation” of 3D images for each acquisition time point, which provides a 3D surface that models the surface of the organ of interest (left ventricular endocardium, aorta lumen). Multiple strategies are being investigated to accomplish this step.

VMTK segmentation: using an open-source software available at www.vmtk.org, which provides a widely used and accepted implementation of the level-set method for image segmentation, we designed a robust segmentation protocol for time-resolved MRI. The objectives of this task are (a) obtain a segmented surface that is an accurate model of the actual surface of the tissue detected by the images in each time frame; (b) guarantee that the deformation of the segmented surfaces that can be detected from phase to phase is merely due to the motion of the vascular structure and not to an “artificial” motion introduced by the segmentation.

Multiscale model segmentation: we implemented, through a in-house Matlab (The Mathworks, Natick, MA) based code, the “active contour model”. This segmentation algorithm is based on the minimization of an energy functional, which is composed of the sum of a local component and a global component. The local component uses a Gaussian kernel to weight the influence of the energy of neighbor pixels around a single pixel over the domain. This local fitting energy drives the level set contour to an edge. The global fitting term uses the average image intensities inside and outside the contour to drive a contour towards an edge.

Good initial results have been achieved using this algorithm and it will be used in the validation of the motion reconstruction.

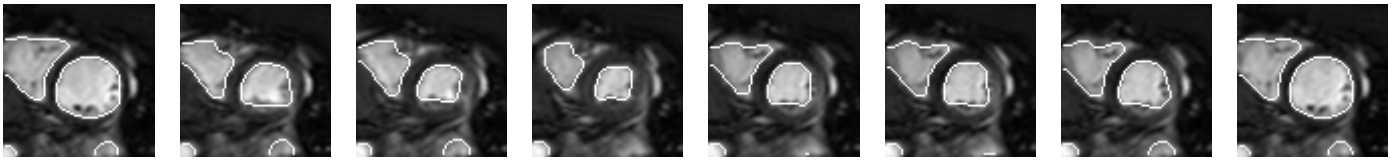

Figure 21. Segmentation of the left ventricle generated using the multiscale active contour model

Both the described algorithms to segment time-resolved images will be validated against marker positions in a ventricle phantom experiment, as detailed in section 3 of this specific aim. Upon successful validation, the protocol that is best performing will be applied to volunteers and patient images acquired for the grant.

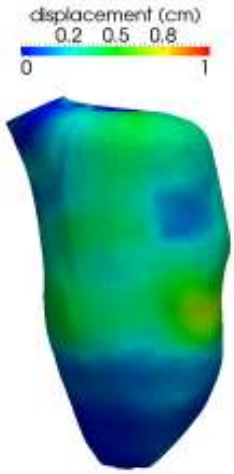

Figure 22. Displacement of the endocardium of the left ventricle at 35th acquisiton acquistion

2. Reconstruction of the ventricle motion from cardiac MRI images

In order to perform CFD simulation on patient-specific geometries, one of the steps that needs to be performed is the reconstruction of the displacement experienced by the endocardium during the cardiac cycle. To this aim, the acquired MRI images have to be processed using a *tracking* (also called *registration*) algorithm. The algorithm that we are employing for this task is an optimization-based surface registration algorithm [25,26] that processes 3D surfaces corresponding to the endocardium at each acquisition time, previously obtained from the segmentation of each stack of images.
Given M+1 triangulated surfaces corresponding to M+1 time frames, the tracking process consists of M registration steps between each consecutive time step. Within each stage, the displacement field for each point of the surface triangulation is obtained, describing the vessel wall motion at the instants of the image acquisition. This displacement between two consecutive frames is computed by minimizing a function that takes into account a proper distance between the two surfaces and a regularizing term, which improves the mathematical properties of the minimization problem and filters out unphysical solutions.

The software to perform the registration is an in-house Matlab-based (The Mathworks, Natick, MA) code, courtesy of M. Piccinelli (Emory University) and E. Haber (University of British Columbia).
The input of the algorithm is a set of segmented surfaces (60 in our case) while the output is the surface motion in time. The displacement of the endocardium at the 35th acquisition is displayed in Figure 22. However, in some regions an abnormal and non-physical motion is detected because the registration process strongly depends on the accuracy of the segmented surfaces available for all the phases. The preliminary results obtained in this case show that if the images are noisy or if the segmentation method employed is heavily operator-dependent, an unphysical artificial motion can be detected. An example of this phenomenon is shown in Figure 23. To overcome this problem, a different method of image segmentation is being investigated. Moreover, the results obtained with various segmentation protocols and this registration approach will be validated against an *in vitro* experiment in the MRI scanner.

3. Motion Reconstruction Validation

The development of clinically applicable fluid-structure interaction (FSI) models of the left heart is inherently challenged when using *in vivo* data for validation, due to the lack of a well-controlled system where detailed measurements of the ventricular wall motion and flow field are available *a priori*. Further, validation of methods used to reconstruct ventricular wall motion from medical imaging data against higher spatiotemporal resolution measurements is necessary. We addressed these challenges through the development of a magnetic resonance imaging (MRI) compatible left ventricle (LV) physical model. The membrane motion

reconstruction method will be used as a gold standard for the validation of the MRI endocardial motion reconstruction methodology using the *in vitro* left heart simulator in the MRI.

Experiments were conducted for heart rate of 70 bpm, 100 mm Hg mean aortic pressure, and cardiac output of 3 L/min. Wall motion measurements were obtained using stereo-photogrammetry (SP) and cine-MRI (Figure 24).

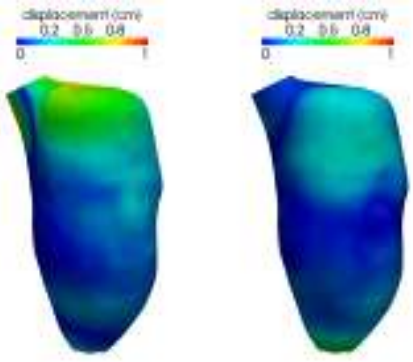

Figure 23. Example of non-physiological displacements on the base of the ventricle at the 31th acquisition (left) and on the apex at the 32nd acquisition (right)

Dual camera stereo-photogrammetry was performed using two high-speed monochromatic cameras (Model A504K, Basler Vision Technologies, Exton, PA) with Nikon macro lenses (60 mm, f2.8; Nikon, Melville, NY). A 4 mm by 4 mm grid was projected onto one side of the outer surface of the ventricle using an industrial strength sharpie pen. The ventricular wall motion was also analyzed using cine magnetic resonance (CMR) imaging. The ventricle was examined using a 3T Siemens scanner. LV motion was acquired using a cine balanced steady-state free precession (bSSFP) sequence. The acquisition sequence was ECG-gated using an eternal TTL pulse sent to an ECG-pulse box which triggered the MRI scanner. The SSFP cine images were acquired with an in-plane resolution of 1.1719 by 1.1719 mm, a slice thickness of 6mm, and a temporal resolution of 7ms. 15 slices were acquired with 0 mm spacing between slices.

Figure 26 compares the normalized volume flux through the LV calculated from CMR and SP. The normalized LV volume flux through the cardiac cycle computed from cine-MRI data matched closely to that from SP, thereby validating the MRI segmentation method. The qualitative trends through the cardiac cycle were similar. The mean discrepancy between CMR and SP was 5.5 ± 3.7% while the largest discrepancy throughout the entire cardiac cycle was approximately 14%, occurring during peak diastole and peak systole.

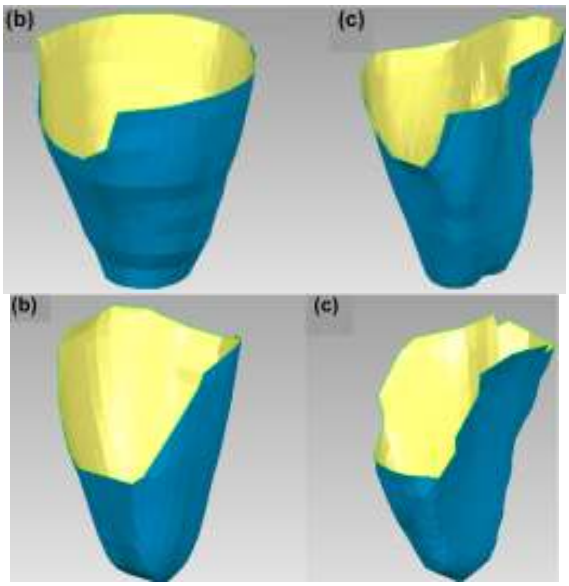

Figure 24. (top) High-speed SP measurements with 3D reconstruction obtained during peak diastolic and peak systolic phases. (bottom) the 3D geometry obtained during peak diastolic and peak systolic phases, respectively, following segmentation and registration of the raw MRI data.

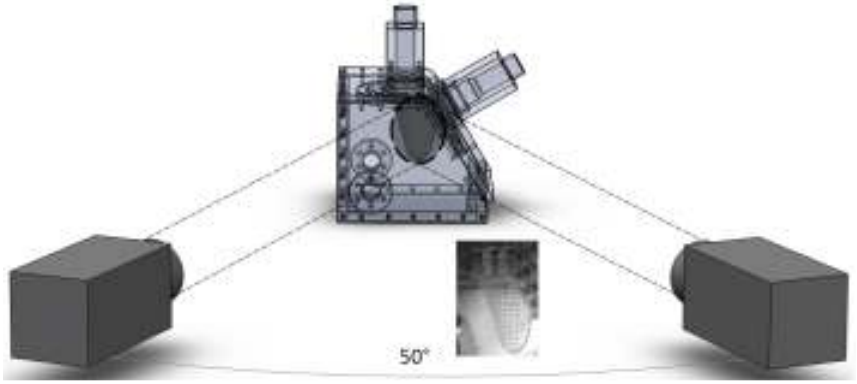

Figure 25. Experimental setup used for SP

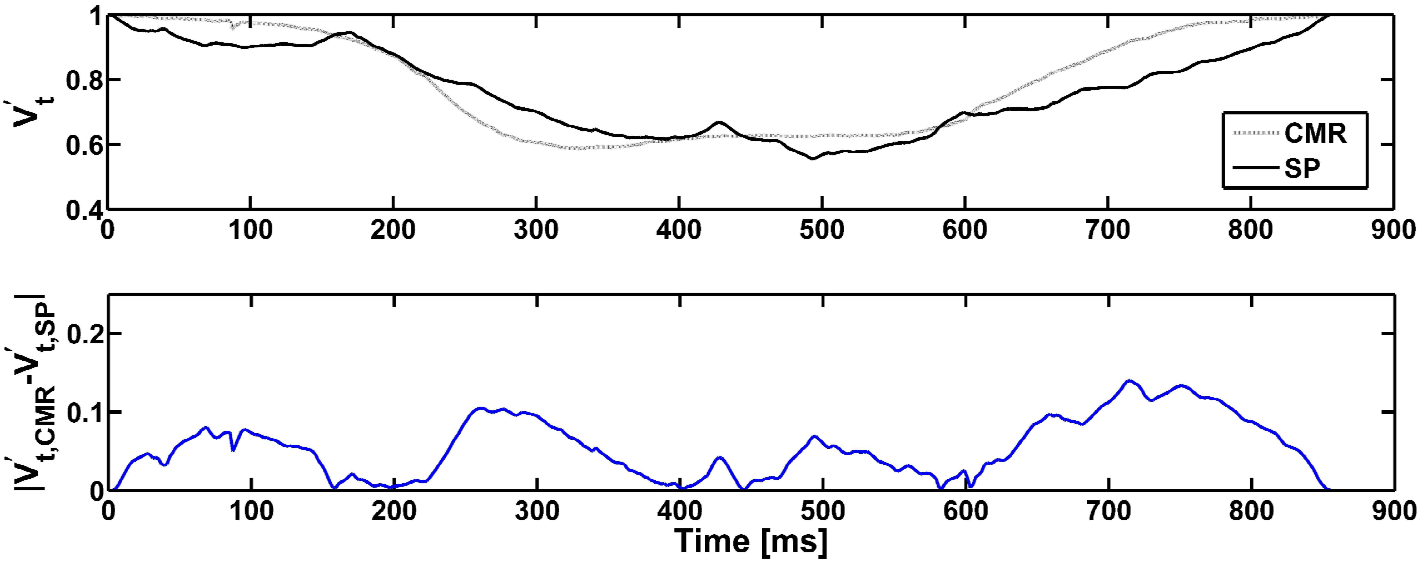

Figure 26. Top: Comparison of the normalized volume flux within the LV physical model obtained using volume reconstruction from stereo-photogrammetry and cine-MRI modalities. Bottom: Absolute errors between CMR and SP reconstructed volume through the cardiac cycle

SPECIFIC AIM IV: Initial application of the computational tools for patient simulation and analysis

The work to date on Specific aim IV is directly related to the progress in each aim mentioned above. The FSI-CFD method has been developed and we have begun to experimentally validate the CFD tool used resolve the intra-ventricular flow, pressure, and SJM leaflet kinematics at the aortic position. We have validated the membrane motion reconstruction methodology to the hemodynamic volume flux thorough the mitral orifice and the out of the aortic outlet.

1. MRI Data Acquisition:

We have scanned four patients with an SJM bileaflet heart valve implanted in the aortic position. The *in-vivo* images of the motion of the endocardial boundary over an entire cardiac cycle were obtained through a set of short axis cine images. The sequence used to acquire the LV motion was an ECG-gated, segmented cine bSSFP technique. The SSFP cine images, at 60 time points in the cardiac cycle were acquired with an in-plane resolution of 1.5 x 1.5 mm with a slice thickness of 10 mm. Images were acquired during an end expiration breath-hold of 8 - 10 seconds.

PCMRI was used to measure the bulk flow at upstream of the mitral valve and downstream of the aortic valve. The position of the imaging plane for the mitral flow was oriented along the mitral annulus. The aortic flow imaging plane was oriented just downstream of the sino-tubular junction. Both flows were acquired at 24 time points in the cardiac cycle using a retrospective ECG-gated gradient echo PC MRI sequence during an end expiration breath-hold.

The pre-processing of the MRI data set was done using an in-house MATLAB (MathWorks, Natick MA) code and visualization done using Paraview (Kitware, open source). As expected, the resolution of the

MRI data set is not high enough to capture vortices as seen in the experimental results; however, it is good enough to pick out bulk flow features. The acquired time series was registered such that a smooth transition between time points occurred. The entire 60-phase time series was then input into the CFD-FSI solver along with the flow through the mitral and aortic valves as boundary conditions.

2. VORTEX RING FORMATION IN ANATOMIC LEFT VENTRICLE

2.1 Hemodynamics of left ventricle with animated kinematics

After we successfully validated our numerical framework for different complex geometries, we carry out the first simulation of intraventricular hemodynamics in an animated left ventricle. The original left ventricle geometry is obtained from MRI data of a volunteer. In this section we apply the kinematic model as described in section 2 to animate the motion of the LV during diastole.

Blood is simulated as an incompressible, Newtonian fluid with dynamic viscosity of $u=3.35\ \ 10^{-6}$ m^2/s and thus its motion is governed by the unsteady, three-dimensional Navier-Stokes equations. The moving LV surface is discretized with an unstructured grid and is immersed in a background, stationary, curvilinear grid of size 201 x 201 x 193. The LV surface is treated as a sharp interface using the Curvilinear Immersed Boundary (CURVIB) method (Ge and Sotiropoulos, 2007). The governing equations are discretized via second-order accurate finite-difference formulas and integrated in time using an efficient, second-order accaurate fractional-step method (Borazjani et al., 2008a). The cardiac cycle in our simulation is T=1.15s, corresponding to a physiologic heart rate of 52 beats per minute.

The mitral inflow waveform used in the simulation, which is indicative of the LV wall kinematics obtained from our model, is used to specify the time-dependent blood flow flux from the left atrium to the LV chamber as boundary condition at the mitral orifice $Q_m = Q_m(t)$. We assume uniform flow distribution at the mitral orifice, which is broadly similar to the natural conditions during diastole. Since the simulations reported herein are carried out only during diastole, the aortic valve is kept fully closed by setting the flow rate through the aorta equal to zero at all times. Finally, the time-dependent LV wall motion is animated via the kinematic model as previously described. This cell-activation model is used to drive the LV blood flow through the no-slip and no-flux boundary conditions that are imposed for the velocity field at the LV wall.

During the diastolic phase the intraventricular flow is dominated by the filling of blood flow from the left atrium into the left ventricular chamber. At initial phase of the E-wave filling, we observe the existence of a large well-defined vortex ring formed at the edge of the mitral orifice as seen in **Error! Reference source not found.**. Since the mitral orifice has a circular shape, the mitral vortex ring has the initial doughnut-shape vorticity distribution around the main's ring circumference. After the E-wave, this vortex ring is fully formed and propagates toward the LV apex.

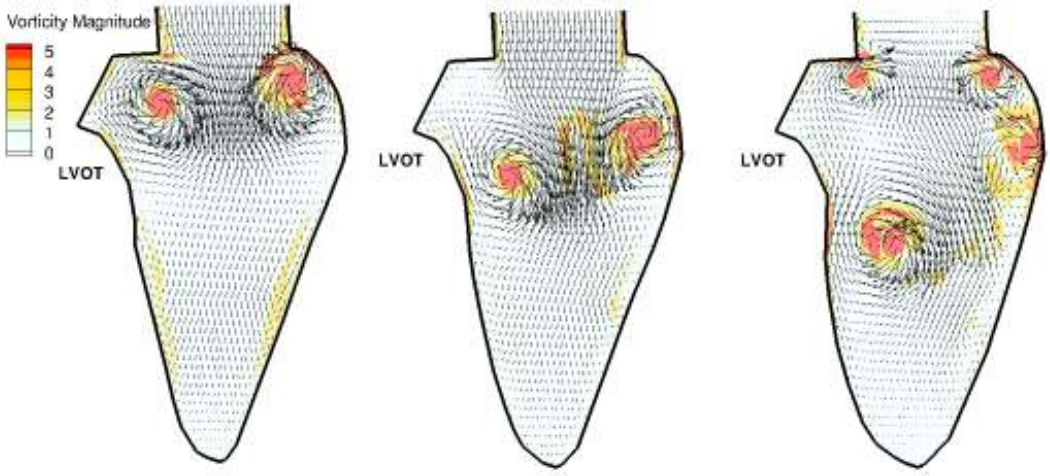

Figure 6 The evolution of the mitral vortex ring during different stages in diastole. The flow is visualized by the velocity vectors superimposed on the contours of non-dimensional vorticity contour. LOVT is the acronym of the Left Ventricle Outflow Tract.

The calculated three-dimensional vortical structures are visualized in **Error! Reference source not found.** in terms of an instantaneous iso-surface of the vorticity magnitude. As seen in **Error! Reference source not**

found., the mitral vortex ring (MVR) has a variable core diameter and begins to interact with the basal geometry shortly after it forms. This interaction causes vorticity to be extracted from the wall and induces the formation of secondary vortex tubes, denoted as trailing vortex tubes that grow from the wall and wrap around the primary ring clearly on during diastole. Moreover, the ring starts to become inclined and propagates toward the posterior wall. The second phase of the MVR evolution is characterized by the stretching and elongation of the secondary vortex tubes, which, while remaining attached to the wall, are seen to wrap around the core of the MVR giving rise to the growth of twisting instabilities along the ring core. At the end of diastole, the MVR impinges on the LV wall and begins to break down into small-scale structures.

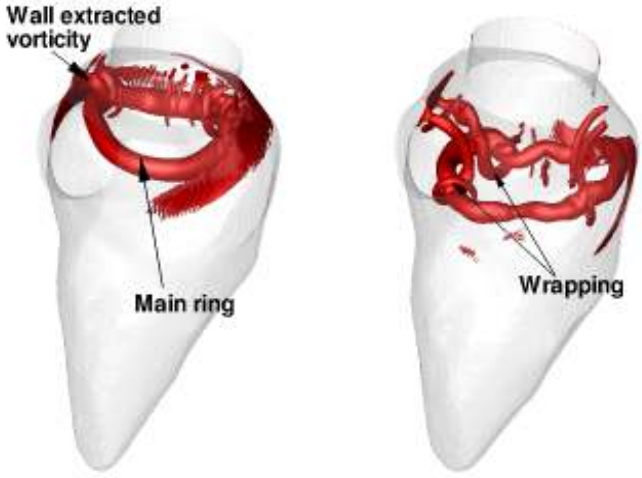

Figure 7 The evolution of the mitral vortex ring. The flow is visualized by the non-dimensional vorticity magnitude.

In brief, our results on the vortex ring formation inside left ventricle reveal a complex, three-dimensional vortical structure consisting of the main ring and pairs of secondary vortex tubes wrapping around the main ring's core. The trailing vortex tubes originate from the heart wall and strech and twist around the MVR's circumference, inducing twisting instabilities to grow and propagate along the ring's circumference. The impingement of the MVR of the LV wall and its subsequent breakup leads to a turbulent-like state at the end of diastole. The details of the computational results are presented in the European Journal of Mechanics B/Fluids (Le and Sotiropoulos, 2012b).

2.2 Vortex ring formation in a patient-specific beating left ventricle

We reconstruct the motion of the left ventricle from a continuous series data of a patient on a whole cardiac cycle. The medical image is from Magnetic Resonance Imaging data with 23 frames over one cardiac cycle. The systolic phase accounts for 38% of the cardiac cycle. All the images are processed by the open-source software VMTK.

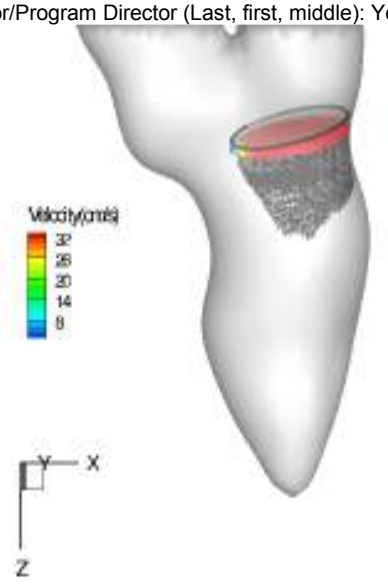

Figure 29. The reconstructed geometry from MRI data at early diastole. The measured plane is at the mitral valve tip indicated by the position of velocity vectors.

The computational domain is a rectangular block following LV shape (shown in **Error! Reference source not found.**). The grid is a structured grid of size 241 x 241 x 241. The grid point is distributed uniformly along all directions. The computational block is approximately aligned to the LV axis an angle of 30 degree. The LV surface, which is represented as a triangular surface, is considered as an immersed boundary inside the computational box. The inflow is set at the measured plane inside the mitral opening. From the MRI data, we can estimate the opening are of the mitral orifice with the maximum circular opening diameter D=32 mm. The profile of the incoming flow is a nearly uniform. Therefore we assume that the incoming flow is orthogonal to this plane following the MRI data and its distribution is uniformly across the mitral orifice at all times. The peak E-wave velocity is determined as U=0.45 m/s and the corresponding Reynolds number is 5023. The cardiac cycle (T) is divided into 1000 timesteps. Since the cardiac cycle is 0.81 s (74bpm), the time step is thus 0.81 ms.

The motion of the LV endocardium is shown in **Error! Reference source not found.**. The LV twist in the clockwise direction during systole (from t/T=0.1 to t/T = 0.333). During that time, the largest velocity is at the apex (shortening along the LV axis). The shortening of the LV wall is monitored on the apical, medial and basal region of the LV. The results show that the basal region does not displace significantly along the main LV axis during the cardiac cycle (just about 1 mm). The apical region displaces the largest (in the order of 9 mm). The medial region displacement is in the order of 4 mm. The shortening along the LV axis is largest at the apex and decreases along the LV axis to the base.

At late systole (t/T > 0.3) the endocardial velocity reduces over the whole endocardium. However, the mid-region still exhibits significantly high velocity magnitude. During diastole (t/T>0.333), the LV untwists in the counter-clockwise direction. Overall the largest velocity (in the mid-region) is in the order of 10cm/s.

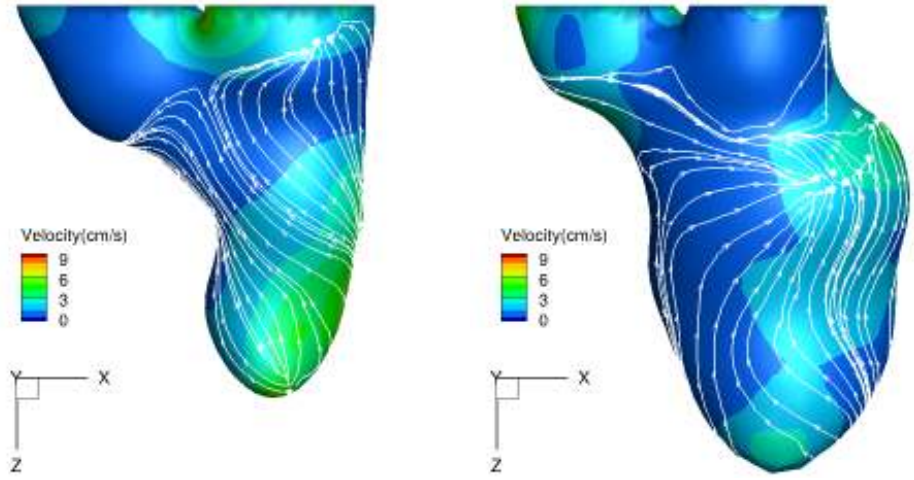

Figure 30. The surface velocity on the endocardium at peak systole (left) and peak diastole (right). The streamlines denote the velocity field for the twist (during systole) and untwist (during diastole).

The main flow structure is shown in **Error! Reference source not found.**. After the E-wave, an inclined vortex is formed near the outflow tract. Due to the inclination of the incoming flow, the vortex core is much larger than the counterpart. During its formation, it interacts with the septal wall and extracts vorticity from the wall. This extraction induces a jet formed on the septal wall (denoted by positive vorticity) toward the mitral plane. During diastasis, the negative vorticity grows. The expansion of the LV in the mid-region also annihilates the positive core to displace toward the posterior wall. Here the role of LV wall motion is most distinctive. Due to the wall motion, the jet is now directed toward the posterior wall. At late E-wave, the sudden expansion of the wall displaces the vortex core toward the posterior wall and the negative core is shifted toward the center of the orifice. Finally, the positive core impinges on the wall but stays intact on the LV wall. During the A-wave, the A-wave vortex ring forms but stay close to the mitral valve's tip. Inside the LV chamber, the core's breakups lead to a number of vortices inside the chamber at the late diastole. These vortices all propagate toward the LV apex. However, they dissipate along the way as well as interact with the LV moving wall. The region near the apex is not covered by vortices during the filling phase. It is rather a separate region due to the large shortening along the LV axis mostly.

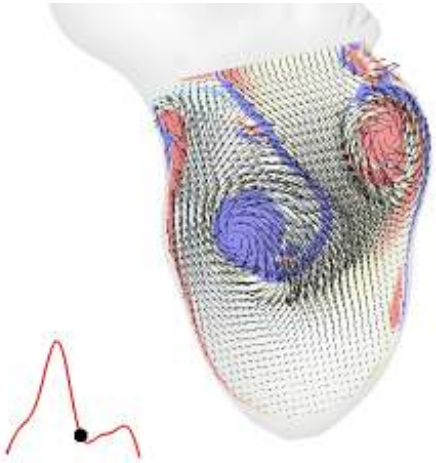

Figure 31. Vortex formation inside the left ventricle during diastasis. The flow is visualized in the main plane (x=0) using out-of-plane vorticity and in-plane velocity vectors

The three-dimensional structure of the flow is shown in **Error! Reference source not found.**. After the E-wave filling, a well-defined vortex ring is formed the mitral plane. As seen in **Error! Reference source not found.**, the core near the septal wall fully separates from the wall. However, the core near the posterior wall still attaches to the mitral's valve tip. The large expansion of the mid-region (see **Error! Reference source**

not found. for the LV wall motion) forces the vortex ring to migrate toward the LV center. It is noteworthy that the vortex ring now has a near rectangular shape with the larger core near the septal wall. Complex vortex tubes connect to the main ring and extend upstream toward the mitral plane. At the end of E-wave, the vortex ring now exhibits the twisting. The twisting first starts by the trailing vortex tube around the main ring. Such large scale twisting continues to grow and the main ring is completely broken up at the end of diastasis leading to smaller vortex tubes to form inside the LV chamber.

Figure 32. The vortex ring formation during E-wave visualized by Q-criteria inside the patient-specific left ventricle. Rich vortex dynamics is found during diastolic filling

3. Fluid structure interaction simulation of an aortic BMHV in patient-specific left ventricle

Previous FSI simulations of heart valves have been carried out in a stand-alone aorta with a prescribed inflow waveform. Recent findings, however, do suggest that the patient-specific flow in the left ventricle outflow tract (LVOT) is greatly affected by the dynamically deforming left ventricle during diastole (Hong et al., 2008; Nakamura et al., 2006). Computational methods for simulating the flow in anatomic LV models reconstructed from imaging modalities have recently been reported but in such models the heart valves have been omitted and their function has been approximated by prescribing appropriate flow wave forms at the mitral valve (MV) and/or aortic valve (AV) positions (Krittian et al., 2010; Schenkel et al., 2009a). In this section, we summarize our recent fluid-structure interaction (FSI) simulations of a bi-leaflet mechanical heart valve (BMAV) implanted in an anatomic LVOT and driven by the dynamic motion of a beating LV (Le, 2011, 2012; Le and Sotiropoulos, 2012b; Le et al., 2012).

A conceptual sketch of our model is shown in **Error! Reference source not found.**. The domain consists of two sub-domains: the LV and the aorta sub-domains, respectively. The numerical method used for the simulations is the FSI-CURVIB method described in detail in (Borazjani et al., 2008b) enhanced with an overset Chimera grid approach to facilitate the accurate discretization of the LV/LVOT sub-domains. The LV moves with prescribed motion (see below) and is treated as a sharp interface immersed boundary. The LVOT and aorta are discretized by a curvilinear boundary fitted mesh and aortic wall is assumed to be rigid. The BMAV is treated as an immersed boundary in the aortic lumen and its motion is calculated via the strongly coupled FSI approach of (Borazjani et al., 2008b). The details of the overall formulation can be found in (Le, 2011) and (Le, 2012).

To simulate the LV motion, we animate an anatomic LV chamber geometry, reconstructed from MRI data of a healthy volunteer, by developing a lumped modeling approach. This approach, which is described in detail in (Le, 2011) and (Le and Sotiropoulos, 2012b), is broadly inspired by cardiac electro-physiology and yields global LV kinematics that are well within the physiological range. The long and short LV axes length of the left ventricle model are L = 80mm and DL = 47mm, respectively. The diameter of the aorta at the LVOT is D = 26.7 mm. No mitral valve is included in the model and thus the mitral orifice is set to be fully open during diastole and fully closed during systole. The effect of the MV is accounted for by imposing a physiologic flow waveform. The heart beat cycle T is chosen to correspond to a heart rate of 52 bpm, T = 1.15s. The simulation time step is Δt = 0.1074 ms and the computational mesh consists of 17.67 million grid nodes. The

valve is a St. Jude Regent 23mmm implanted in the LVOT.

During early diastole **Error! Reference source not found.**a, the LV flow is dominated by small scale vortical structures following the breakdown of the E- and A-wave mitral vortex rings during systole (see (Le, 2011; Le and Sotiropoulos, 2012b; Le et al., 2012) for more details). The large scale flow direction in the LV rotates in the clockwise direction, guiding the blood flow into the LVOT. The systolic phase starts with the contraction of the LV causing the small scale flow structures to be ejected into the LVOT and the resulting accelerating flow through the LVOT to open the valve leaflets as shown in **Error! Reference source not found.**b. Shear layer formation and roll-up phenomena are clearly observed in **Error! Reference source not found.**b in the wake of the valve leaflets. These shear layers are broadly similar to those observed in previous simulations and experiments with a BMHV in a straight axi-symmetric aorta (Dasi et al., 2007). Our results do show, however, that in the anatomic case the shear-layer formation is impacted by interactions with small-scale flow structures that are advected by the accelerating systolic flow from the LV chamber past the valve leaflets. As the LV continues to contract, the vortical structures shed from the valve leaflets advance toward the aortic root and break up rapidly into a turbulent-like state past peak systole. The three-dimensional structure of the flow phenomena described above is illustrated in **Error! Reference source not found.**, which shows the formation of the asymmetric, donut-shaped, mitral vortex ring at the end of the E-wave filling. The subsequent breakdown of this ring at late diastole and the intense stretching of vertical structures as the contracting LV directs the flow into the LVOT and opens the valve. The details of the computation can be found in our paper in the Journal of Computational Physics (Le and Sotiropoulos, 2012a).

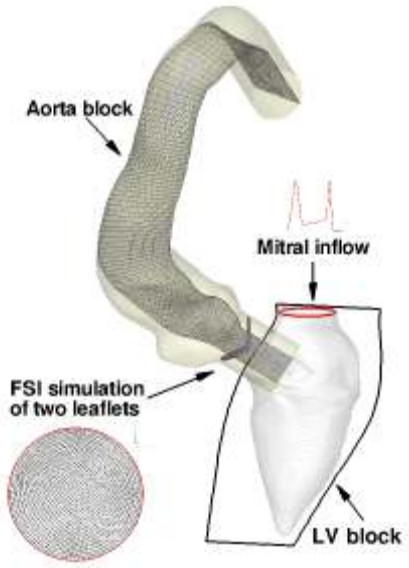

Figure 33. a)The computational grid consists of two distinct blocks: the left ventricle block and the aorta block. The left ventricular block is a structured grid of size 161 x 281 x 161. For clarity, the 3D background grid is shown only on the symmetry plane of the BMHV for every four grid line. The aorta block is a body fitted mesh of size 161 x 161 x 401. For clarity, every one out of four grid points is shown. At the mitral position, uniform pulsatile flow Q_m (t) is specified as boundary condition and the mitral valve is assumed to be fully open during diastole.

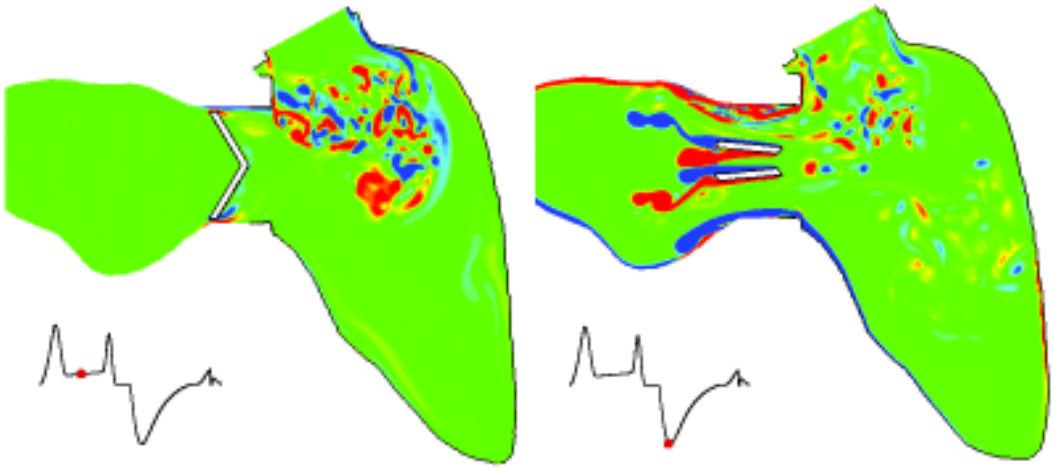

Figure 34. The formation and breakup of mitral vortex rings during diastole (left). The BMHV opens at the peak systole and induces the unstable shear layer to form on the leaflet surfaces (right). The flow is visualized using the out-of-plane vorticity on the symmetry plane of the BMHV. The red dot in the inset shows the time instance in the cardiac cycle.

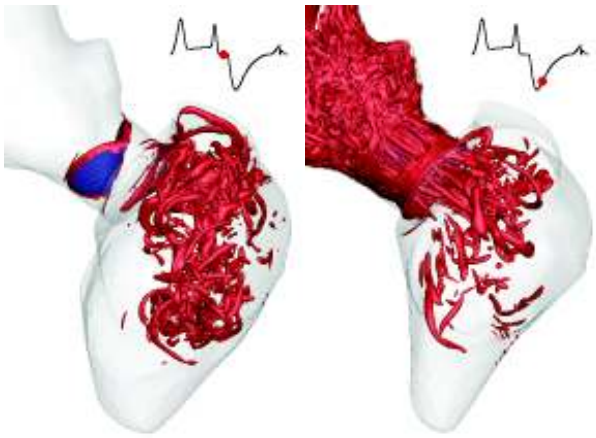

Figure 35. The formation of coherent structures inside the left ventricular chamber during diastole in (a) and (b). The small scale structures are advected into the aorta during systole in (c) and (d). The flow is visualized by Q-criteria (Hunt et al., 1988). The view is from the apex. The red dot in the inset shows the time instance in the cardiac cycle.

REFERENCES

Beyar, R., and Sideman, Samuel, 1986, The dynamic twisting of the left ventricle: A computer study: Annals of Biomedical Engineering, v. 14, p. 547-562.

Beyar, R., and S. Sideman, 1984,, A computer study of the left ventricular performance based on fiber structure, sarcomere dynamics, and transmural electrical propagation velocity: Circ Res, v. 55, p. 358-375.

Borazjani, I., L. Ge, and Sotiropoulos, Fotis, 2008a, Curvilinear immersed boundary method for simulating fluid structure interaction with complex 3D rigid bodies: Journal of Computational Physics, v. 227, p. 7587 - 7620.

Borazjani, I., L. Ge, and F. Sotiropoulos, 2008b, Curvilinear immersed boundary method for simulating fluid structure interaction with complex 3D rigid bodies: Journal of Computational Physics, v. 227, p. 7587-7620.

Chadwick, R., 1982, Mechanics of the left ventricle: Biophysical Journal, v. 39, p. 279 - 288.

Dasi, L. P., L. Ge, H. A. Simon, F. Sotiropoulos, and A. P. Yoganathan, 2007, Vorticity dynamics of a bileaflet mechanical heart valve in an axisymmetric aorta: Physics of Fluids, v. 19.

Ge, L., and F. Sotiropoulos, 2007, A numerical method for solving the 3D unsteady incompressible Navier-

Stokes equations in curvilinear domains with complex immersed boundaries: Journal of Computational Physics, v. 225, p. 1782.

Hong, G. R., G. Pedrizzetti, G. Tonti, P. Li, Z. Wei, J. K. Kim, A. Baweja, S. Z. Liu, N. Chung, H. Houle, J. Narula, and M. A. Vannan, 2008, Characterization and Quantification of Vortex Flow in the Human Left Ventricle by Contrast Echocardiography Using Vector Particle Image Velocimetry: Jacc-Cardiovascular Imaging, v. 1, p. 705-717.

Hunt, J. C. R., A. A. Wray, and P. Moin, 1988, Eddies, stream, and convergence zones in turbulent flows: Center for Turbulence Research Report CTR-S88, p. 193-208.

Hunter, P. J., A. J. Pullan, and B. H. Smaill, 2003,, MODELING TOTAL HEART FUNCTION: Annual Review of Biomedical Engineering, v. 5, p. 147-177.

Kim, W. Y., P. G. Walker, E. M. Pedersen, J. K. Poulsen, S. Oyre, K. Houlind, and Yoganathan, Ajit P, 1995, Left ventricular blood flow patterns in normal subjects: A quantitative analysis by three-dimensional magnetic resonance velocity mapping: Journal of the American College of Cardiology, v. 26, p. 224 - 238.

Krittian, S., U. Janoske, H. Oertel, and T. Bohlke, 2010, Partitioned Fluid-Solid Coupling for Cardiovascular Blood Flow: Annals of Biomedical Engineering, v. 38, p. 1426-1441.

Le, T. B., 2011, A computational framework for simulating cardiovascular flows in patient-specific anatomies, University of Minnesota, 205 p.

Le, T. B., 2012, Fluid-structure interaction of an aortic heart valve prosthesis driven by electrical excitation of a patient-specific left ventricle: Journal of Computational Physics, v. Accepted with minor revisions.

Le, T. B., I. Borazjani, S. Kang, and F. Sotiropoulos, 2011, On the structure of vortex rings from inclined nozzles: Journal of Fluid Mechanics, v. 686, p. 451-483.

Le, T. B., and F. Sotiropoulos, 2012a, Fluid-structure interaction of an aortic heart valve prosthesis driven by an animated anatomic left ventricle: Journal of Computational Physics, v. http://dx.doi.org/10.1016/j.jcp.2012.08.036

Le, T. B., and F. Sotiropoulos, 2012b, On the three-dimensional vortical structure of early diastolic flow in a patient-specific left ventricle: European Journal of Mechanics- B/Fluid, v. 35, p. 20-24.

Le, T. B., F. Sotiropoulos, D. Coffey, and D. Keefe, 2012, Vortex Formation and Instability in the Left Ventricle: Physics of Fluids, v. in press.

Nakamura, M., S. Wada, and T. Yamaguchi, 2006, Computational analysis of blood flow in an integrated model of the left ventricle and the aorta: Journal of Biomechanical Engineering, v. 128, p. 837-43.

Saber, N., A. D. Gosman, N. Wood, P. Kilner, C. Charrier, and D. Firmin, 2001, Computational Flow Modeling of the Left Ventricle Based on In Vivo MRI Data: Initial Experience: Annals of Biomedical Engineering, v. 29, p. 275-283.

Schenkel, T., M. Malve, M. Reik, M. Markl, B. Jung, and H. Oertel, 2009a, MRI-based CFD analysis of flow in a human left ventricle: methodology and application to a healthy heart: Annals of Biomedical Engineering, v. 37, p. 503-15.

Schenkel, T., M. Malve, M. Reik, M. Markl, B. Jung, and H. Oertel, 2009b, MRI-Based CFD Analysis of Flow in a Human Left Ventricle: Methodology and Application to a Healthy Heart: Annals of Biomedical Engineering, v. 37, p. 503-515.

Thomas, J. D., and AE, Weyman, 1991, Echocardiographic Doppler evaluation of left ventricular diastolic function. Physics and physiology: Circulation, v. 84, p. 977-990.

Troolin, D. R., and E. K. Longmire, 2010, Volumetric velocity measurements of vortex rings from inclined exits: Experiments in fluids, v. 48, p. 409-420.

Webster, D. R., and E. K. Longmire.

Wu, J., Yun, B.M., Fallon, A.M., Hanson, S.R., Aidun, C.K., and Yoganathan, A.P., 2011. Numerical Investigation of the Effects of Channel Geometry on PLatelet Activation and Blood Damage: Annals of Biomedical Engineering, v. 39, p. 897-910

Yun, B.M., Wu, J., Simon, H.A., Arjunon, S., Sotiropoulos, F., Aidun, C.K., Yoganathan, A.P., 2012. A numerical investigation of blood damage in the hinge area of aortic bileaflet mechanical heart valves during the leakage phase: Annals of Biomedical Engineering. v. 40, 1468-1485.

Yoganathan, A. P., Z. He, and S. Casey Jones, 2004,, Fluid mechanics of heart valves: Annual Review of Biomedical Engineering, v. 6, p. 331-362.

LIST OF ACCOMPLISHMENTS	GRANT NUMBER HL70262-08	
	PERIOD COVERED BY THIS REPORT	
PRINCIPAL INVESTIGATOR OR PROGRAM DIRECTOR Ajit P. Yoganathan	FROM 07/01/08	THROUGH 06/30/13

APPLICANT ORGANIZATION

Georgia Tech Research Corp.

TITLE OF PROJECT (Repeat title shown in Item 1 on first page)

Computational Modeling of Mechanical Heart Valves

A. Human Subjects (Complete Item 6 on the Face Page)

Involvement of Human Subjects ☒ No Change Since Previous Submission ☐ Change

B. Vertebrate Animals (Complete Item 7 on the Face Page)

Use of Vertebrate Animals ☒ No Change Since Previous Submission ☐ Change

SEE PHS 2590 INSTRUCTIONS.

A short list of significant accomplishments during the 5-year period of the grant is provided below:

- Development and testing of a MRI-compatible left heart simulator using an anatomically realistic, flexible-walled LV physical model; this bridges the gap of the use of *in vitro* platforms to obtain data using both laboratory-level and clinical imaging methods

- First time validation of a cardiac FSI solver incorporating left heart anatomy with moving boundaries, using high-resolution experimental data obtained from laboratory based and imaging based modalities

- Suspension flow simulations of BMHV flows at the highest spatiotemporal resolution to date to evaluate blood damage performance in physiologic and patho-physiologic conditions

- Detailed flow visualization through bileaflet mechanical heart valve (BMHV) hinge regions using micro-scale experimental techniques to elucidate blood damage potential regions

- First time experimental validation of MRI post-processing methods used to reconstruct LV wall motion and flow, using gold standard data obtained from higher spatiotemporal resolution methods

- Use of cardiac MRI data from BMHV patients that are reconstructed to obtain patient-specific wall motion and flow fields; corresponding preliminary patient-specific, FSI simulations of left ventricular flow fields using this data

JOURNAL ARTICLES

1. Santhanakrishnan, A., Okafor, I. U., Chaffins, B., Mirabella, L., Oshinski, J. N., and Yoganathan, A.P., "MRI-compatible Physical Model of the Left Ventricle for Multi-modality Characterization of Wall Motion and Hemodynamics," Submitted to Annals of Biomedical Engineering, 2013.

2. Yun B.M., Dasi L.P., Aidun C.K., and Yoganathan A.P., “Computational modeling of flow through bileaflet mechanical heart valves using the lattice-Boltzmann method,” Submitted to Journal of Fluid Mechanics, 2013.

3. Yun B.M., Dasi L.P., Aidun C.K., and Yoganathan A.P., “Highly resolved flows through prosthetic heart valves using the lattice-Boltzmann method,” Submitted to Journal of Fluid Mechanics, 2013.

4. Jun, B.H., Yoganathan, A.P., and Saikrishnan, N., “In Vitro Micro Particle Image Velocimetry Measurements in the Hinge Region of a St. Jude Medical® Regent™ Bileaflet Mechanical Heart Valve,” Submitted to Annals of Biomedical Engineering, 2013.

5. Borazjani, I., Ge, L., Le, T., and Sotiropoulos, F., ”An overset immersed boundary framework for simulating complex 3D flow,” Computer and Fluids, vol. 77, pp. 76-96, 2013. PMID: 23833331.

6. Votta, E., Le, T. B., Stevanella, M., Fusini, L., Caiani, E. G., Redaelli, A., and Sotiropoulos, F., ”Toward patient-specific simulations of cardiac valves: state-of the art and future directions,” Journal of Biomechanics, vol. 46(2), pp. 217-228, 2013. PMID: 23174421.

7. Le, T. B., and Sotiropoulos, F., ”Fluid-structure interaction of an aortic heart valve prosthesis driven by an animated anatomic left ventricle,“ Journal of Computational Physics, vol. 244, pp. 41-62, 2012. PMID: 23729841.

8. Le, T., Sotiropoulos, F., Coffey, D., and Keefe, D., “Vortex Formation and Instability in the Left Ventricle,” Physics of Fluids, vol. 24, pp. 91110, 2012. PMID: 23112565.

9. Yun, B.M., Wu, J., Simon, H.A., Arjunon, S., Sotiropoulos, F., Aidun, C.K., and Yoganathan, A.P., “A Numerical Investigation of Blood Damage in the Hinge Area of Aortic Bileaflet Mechanical Heart Valves During the Leakage Phase”, Annals of Biomedical Engineering, vol. 40, no. 7, pp. 1468-1485, 2012. PMID: 22215278.

10. Yap, C.H., Saikrishnan, N., Tamilselvan, G., Yoganathan, A.P., “Experimental Technique of Measuring Dynamic Fluid Shear Stress on the Aortic Surface of the Aortic Valve

Leaflet", Journal of Biomechanical Engineering, vol. 133(6), 061007, 2011. PMID: 21744927.

11. Yap, C.H., Saikrishnan, N., Tamilselvan, G., Yoganathan, A.P., "Experimental Measurement of Dynamic Fluid Shear Stress on the Aortic Surface of the Aortic Valve Leaflet", Biomechanics and Modeling in Mechanobiology, Volume 11, Numbers 1-2, pp. 171-182, 2012. PMID: 21465260.

12. Le, T.B., and Sotiropoulos, F., "On the three-dimensional vortical structure of early diastolic flow in a patient-specific left ventricle," European Journal of Mechanics-B/Fluids, vol. 35, pp. 20-24, 2012. PMID: 22773898.

13. Wu, J., Yun, B.M., Fallon, A.M., Hanson, S.R., Aidun, C.K., Yoganathan, A.P.,"Numerical Investigation of the Effects of Channel Geometry on Platelet Activation and Blood Damage" Annals of Biomedical Engineering, vol. 39, no. 2, pp. 897–910, 2011. PMID: 20976558.

14. Coffey, D., Malbraaten, N., Le, T. B., Borazjani, I., Sotiropoulos, F., Erdman, A. G., and Keefe, D. F., "Interactive Slice WIM: Navigating and Interrogating Volume Datasets Using a Multi-Surface, Multi-Touch VR Interface," IEEE Transactions on Visualization and Computer Graphics, vol. 18, no. 10, pp. 1614-1626, 2011. PMID: 22144526.

15. Le, T. B., Borazjani, I., Kang, S., and Sotiropoulos, F., "On the structure of vortex rings from inclined nozzles," Journal of Fluid Mechanics, vol. 686, pp. 451-483, 2011.

16. Borazjani, I., and Sotiropoulos, F., "The effect of implantation orientation of a bi-leaflet mechanical heart valve on kinematics and hemodynamics in an anatomic aorta," Journal of Biomechanical Engineering, vol. 132, no. 11, pp. 111005, 2010. PMID: 21034146.

17. Yap C.H., Kim H.S., Balachandran, K., Weiler, M,. Haj-Ali, R., Yoganathan, A.P., "Dynamic deformation characteristics of porcine aortic valve leaflet under normal and hypertensive conditions." American Journal of Physiology – Heart and Circulatory Physiology, Vol. 298, No. 2, pp. H395-405, 2010. PMID: 19915178.

18. Murphy, D.W., Dasi, L.P., Vukasinovic, J., Glezer, A., and Yoganathan, A.P., "Reduction of Procoagulant Potential of B-datum Leakage Jet Flow in Bileaflet Mechanical Heart Valves via Application of Vortex Generator Arrays", Journal of Biomechanical Engineering-Transactions of the ASME, Vol. 132(7), pp. 071011:1-10, 2010. PMID: 20590289.

19. Yap, C.H., Dasi, L.P., and Yoganathan, A.P., "Dynamic Hemodynamic Energy Loss in Normal and Stenosed Aortic Valve", Journal of Biomechanical Engineering, Vol. 132(2), pp: 021005:1-10, 2010. PMID: 20370242.

20. Simon, H.A., Ge, L., Sotiropoulos F., and Yoganathan, A.P., “Numerical Investigation of the Performance of Three Hinge Designs of Bileaflet Mechanical Heart Valves,” Annals of Biomedical Engineering. vol. 38, no. 11, pp. 3295-3310, 2010. PMID: 20571852.

21. Simon, H.A., Ge, L., Sotiropoulos F., and Yoganathan, A.P., “Simulation of the Three-Dimensional Hinge Flow Fields of a Bileaflet Mechanical Heart Valve Under Aortic Conditions,” Annals of Biomedical Engineering, vol. 38, no. 3, pp. 841-853, 2010. PMID: 19960368.

22. Dasi, L.P., Simon, H.A., Sucosky, P., and Yoganathan, A. P., “Fluid mechanics of Artificial Heart Valves”, Journal of Clinical and Experimental Pharmacology and Physiology, Vol 36 (2), pp. 225-237, 2009. PMID: 19220329.

23. Dasi, L.P., Simon, H.A. and Yoganathan, A.P., “Artificial heart valve fluid mechanics,” invited review in special series: New Frontiers in Biomedical Engineering, Journal of Clinical and Experimental Pharmacology and Physiology, Vol 36 (2), pp. 225-237, 2009.

24. Borazjani, I., Ge, L., and Sotiropoulos, F., “High resolution fluid-structure interaction simulations of flow through a bi-leaflet mechanical heart valve in an anatomic aorta,” Annals of Biomedical Engineering, vol. 38, no. 2, pp. 326-344, 2009. PMID: 19806458.

25. Sotiropoulos, F., and Borazjani, I., “A Review of the State-of-the-Art Numerical methods for Simulating Flow through Mechanical Heart Valves,” Medical and Biological Engineering and Computing, vol. 47, no. 3, pp. 245-256, 2009. PMID: 19194734.

26. Ge, L., and Sotiropoulos, F., “Direction and Magnitude of Hemodynamic stresses on the Leaflets of Aortic valves: Is there a Link with Valve Calcification,” Journal of Biomechanical Engineering, vol. 132, no. 1, pp. 014505, 2009. PMID: 20524753.

27. Borazjani, I., and Sotiropoulos, F., “Flow-Induced Vibrations of two Cylinders in Tandem in the Proximity-Wake Interference Region,” Journal of Fluid Mechanics, vol. 621, pp. 321-364, 2009.

28. Sotiropoulos, F., Aidun, C., Borazjani, I., and MacMeccan, R., “Computational Techniques for Biological Flows: From Blood-Vessel Scale Hemodynamics to Blood-Cells,” in Image-Based Computational Modeling in the Human Circulatory System (edited by Chandran, Udaykumar, and Reinhardt), Springer Verlag (2009).

29. Borazjani, I., Ge, L., and Sotiropoulos, F., “Curvilinear immersed boundary method for simulating fluid structure interaction with complex 3d rigid bodies,” Journal of Computational Physics, vol. 227, pp. 7587-7620, 2008.

30. Ge, L., Dasi, L. P., Sotiropoulos, F., and Yoganathan, A. P., “Characterization of hemodynamic forces induced by mechanical heart valves: Reynolds vs. viscous stresses,” Annals of Biomedical Engineering, vol. 36, no. 2, pp. 276-297, 2008. PMID: 18049902.

PROCEEDINGS

1. Le T., Borazjani I. and Fotis Sotiropoulos, Direct Numerical Simulation of the intra-ventricular flow inside the human left heart, The 7th International Symposium on turbulence and shear flow phenomena, Ottawa, Canada, July 2011.

2. Borazjani, I., Le, T., Sotiropoulos, F., “Effect of Orientation of a Bi-leaflet Mechanical Heart Valve Implanted in an Anatomic Aorta on Hemodynamics,” 11th-World Congress on Medical Physics and Biomedical Engineering, Munich, Germany, September 2009.

3. Borazjani, I., Le, T., Kang, S., Behara, S., Sotiropoulos, F., “Simulating FSI Problems via the Curvilinear Immersed Boundary Method: From Biofluids to Wind Turbines,” Academy Colloquium on Immersed Boundary Methods, Royal Netherlands Academy of Arts and Sciences, June 2009.

PRESENTATIONS (Abstract only)

1. Santhanakrishnan, A., Okafor, I., Angirish, Y., Yoganathan, A. P., “E□ect of varying heart rate on intra-ventricular filling fluid dynamics,” 66th Annual American Physical Society Division of Fluid Dynamics Meeting, Pittsburgh, PA, November 2013.

2. Okafor, I., Angirish, Y., Yoganathan, A. P., Santhanakrishnan, A., “E□ect of mitral orifice shape on intra-ventricular filling fluid dynamics,” 66th Annual American Physical Society Division of Fluid Dynamics Meeting, Pittsburgh, PA, November 2013.

3. Yun, B.M., Aidun, C. K., Yoganathan, A. P., “Blood Damage Quantification in Cardiovascular Flows through Medical Devices Using a Novel Suspension Flow Method,” ASME/FDA 2013 1st Annual Frontiers in Medical Devices: Applications of Computer Modeling and Simulation, Washington, DC, September 2013.

4. Le, T. B., Gilmanov, A., Stolarski, H., Sotiropoulos, F., “Fluid-structure interaction simulation of cardiovascular tissues: a coupling between a non-linear finite element

model of thin shells with the curvilinear immersed boundary method," COUPLED PROBLEMS, Spain, June 2013.

5. Le, T. B., Gilmanov, A., Stolarski, H., Sotiropoulos, F., "High resolution simulation of tri-leaflet aortic heart valve in an idealized aorta," Design of Medical Devices Conference, Minneapolis, April 2013.

6. Yun, B.M., Aidun, C. K., Yoganathan, A. P., "A Multiphase Flow Methodology For Quantifying Blood Element Damage In Cardiovascular Flows," Computer Methods in Biomechanics and Biomedical Engineering: 11th International Symposium, Salt Lake City, UT, April 2013.

7. Le, T. B., Sotiropoulos, F., Mirabella, L., Chaffins, B., Santhanakrishnan, A., Oshinski, J. N., Yoganathan, A. P., "High-resolution numerical simulation of Left Ventricular Hemodynamics Guided by *in-vivo* Cardiac Magnetic Resonance Data," 65th Annual American Physical Society Division of Fluid Dynamics Meeting, San Diego, CA, November 2012.

8. Gilmanov, A., Stolarski, H., Le, T., Sotiropoulos, F., "A numerical model for simulation fluid-structure interaction problems with large deformations of thin shells," 65th Annual American Physical Society Division of Fluid Dynamics Meeting, San Diego, CA, November 2012.

9. Yun, B. M., Aidun, C. K., Yoganathan, A. P., "Simulations of Pulsatile Suspension Flow Through Bileaflet Mechanical Heart Valves to Quantify Platelet Damage," 65th Annual American Physical Society Division of Fluid Dynamics Meeting, San Diego, CA, November 2012.

10. Yun, B. M., Lee, L., Aidun, C. K., Yoganathan, A. P., "Simulations of Platelet Damage in Bileaflet Mechanical Heart Valve Flows in the Closing Phase," Biomedical Engineering Society: 2012 Meeting, Atlanta, GA, October 2012.

11. Yun, B. M., Aidun, C. K., Yoganathan, A. P., "Simulations of Platelet Damage in Pulsatile Flows through Bileaflet Mechanical Heart Valves with Parameter Variation," Biomedical Engineering Society: 2012 Meeting, Atlanta, GA, October 2012.

12. Chaffins, B., Santhanakrishnan, A., Mirabella, L., Oshinski, J., Yoganathan A.P., "Multi-Modality Motion Analysis of a Magnetic Resonance Imaging Compatible Left Ventricular Phantom", Biomedical Engineering Society: 2012 Meeting, Atlanta, GA, October 2012.

13. Jun, B., Saikrishnan, N., and Yoganathan, A.P., "In Vitro Micro Particle Image Velocimetry Measurement in the Hinge Region of St. Jude Medical® Regent™ Bileaflet Mechanical HeartValve", Biomedical Engineering Society: 2012 Meeting, Atlanta, GA. October 2012.

14. Santhanakrishnan, A., Chaffins, B., Le, T., Okafor, I., Sotiropoulos,F., Yoganathan, A. P., "An Experimental and Computational Study In Left Ventricle Models Examining

Vortex Formation from Inclined Inflownozzles During Diastolic Filling," Biomedical Engineering Society: 2012 Meeting, Atlanta, GA ,October 2012.

15. Chaffins, B., Le, T.B., Santhanakrishnan, A., Mirabella, L., Sotiropoulos, F., Yoganathan, A.P., "Development of an Anatomically Realistic Left Ventricle Physical Model and Multi-Modality Experimental Platform for Validation of Patient-Specific Computational Simulations", 14th Annual Summer Bioengineering Conference of the American Society of Mechanical Engineers, Fajardo, Puerto Rico, June 2012.

16. Yun B.M., Aidun C.K., Yoganathan A.P. "Simulations of Flow Through Bileaflet Mechanical Heart Valves with Asymmetric Leaflet Motion", 14th Annual Summer Bioengineering Conference of the American Society of Mechanical Engineers, Fajardo, Puerto Rico, June 2012.

17. Le, T. B., Chaffins, B., Mirabella, L., Santhanakrishnan, A., Yoganathan, A. P., Sotiropoulos, F., "Experimental and computational studies of the aortic bi-leaflet mechanical heart valve (BMHV) hemodynamics in an idealized left ventricle," 5th Biennial Meeting on Heart Valve Biology and Tissue Engineering, Myconos, Greece, May 2012.

18. Le, T. B., Chaffins, B., Mirabella, L., Santhanakrishnan, A., Sotiropoulos, F., Yoganathan, A. P., "High resolution numerical simulation and experimental studies of left ventricular hemodynamics," ASME Verification and Validation Symposium, Las Vegas, NV, May 2012.

19. Yun, B. M., Dasi, L. P., Aidun, C. K., Yoganathan, A. P., "Simulations of Pulsatile Flow Through Bileaflet Mechanical Heart Valves," The 7th International Symposium on Biomechanics in Vascular Biology and Cardiovascular Disease, Atlanta, GA, April 2012.

20. Le, T., Sotiropoulos, F., "High-resolution numerical simulation of patient-specific hemodynamics with implanted medical devices," Computational Fluid Dynamics (CFD) in Medicine and Biology - Seventh International Biofluid Mechanics Symposium, Ein Bokek, Dead Sea, Israel, March 2012.

21. Le, T., Sotiropoulos, F., Coffey, D., Keefe, D., "Vortex formation and instability in the left ventricle," 64th Annual meeting of APS Division of Fluid Dynamics, Baltimore, MD, November 2011.

22. Le, T., Sotiropoulos, F., "The effect of mitral orifice eccentricity on the left ventricle diastolic flow patterns," 64th Annual meeting of APS Division of Fluid Dynamics, Baltimore, MD, November 2011.

23. Le, T., Sotiropoulos, F., "High resolution simulation of an aortic valve prothesis in patient-specific left heart anatomy," ASME Emerging Technologies the 6th Frontiers in Biomedical Devices Conference & Exhibition, Irvine, CA, September 2011.

24. Yun, B. M., Aidun, C. K., Yoganathan, A. P., "Simulations of Pulsatile Flow Through Bileaflet Mechanical Heart Valves to Assess Platelet Damage," Food and Drug

Administration Workshop: Computational Methods for Cardiovascular Devices, Silver Spring, MD, September 2011.

25. Chaffins, B., Le, T., Mirabella, L., Santhanakrishnan, A., Saikrishnan, N., Sotiropoulos, F., Yoganathan, A.P., “High Resolution Experimental and Computational Study of Flow Through a Bi-leaflet Mechanical Hear Valve (BMHV) in a Model Left Ventricle,” Biomedical Engineering Society: 2011 Meeting, Hartford, CT, October 24, 2011.

26. Le T., Borazjani I., Sotiropoulos, F., “Direct Numerical Simulation of the intra-ventricular flow inside the human left heart,” The 7th International Symposium on turbulence and shear flow phenomena, Ottawa, Canada, July 2011.

27. Le, T., Sotiropoulos, F., “On the effect of oral cavity shape in the efficiency of jet-propelled swimmers,” The IV International Conference on Computational Methods for Coupled Problems in Science and Engineering - COUPLED PROBLEMS, Kos Island, Greece, June 20 – 22, 2011.

28. Le, T., Borazjani, I., Sotiropoulos, F., “A computational framework for high resolution simulations of patient-specific left heart hemodynamics with aortic valve prothesis,” EUROMECH 529 - CARDIOVASCULAR FLUID MECHANICS from theoretical aspects to diagnostic and therapeutic support - CVFM2011, Faculty of Engineering - University of Cagliari, June 2011.

29. Sotiropoulos, F., Le, T., “Patient-Specific Simulation of Cardiac Devices: Recent advances and future challenges,” High Performance Computing Symposium in Medical Science, Montreal, Canada, June 2011.

30. Yun, B. M., Wu, J., Aidun, C. K., Yoganathan, A. P., “Simulations of Flow Through Bileaflet Mechanical Heart Valves to Assess Platelet Damage,” Proceedings of the American Society of Mechanical Engineers (ASME), Farmington, PA, June 2011.

31. Le, T., Sotiropoulos, F., “Evaluation of medical device performances in patient-specific anatomy using high resolution simulation,” 10th Design of Medical Devices Conference, Minneapolis, MN, April 2011.

32. Le T., Borazjani, I., Sotiropoulos, F., “High resolution simulation of the left heart hemodynamics in patient-specific anatomies,” 63rd Annual meeting of APS Division of Fluid Dynamics, Long Beach, CA, November 2010.

33. Yun, M., Wu, J., Simon, H., Sotiropoulos, F., Aidun, C., Yoganathan, A. P., "A Numerical Investigation of Blood Damage in the Hinge Area of Bileaflet Mechanical Heart Valves,” 63rd Annual Meeting of APS Division of Fluid Dynamics, Long Beach, CA, November 2010.

34. Le, T., Borazjani, I., Sotiropoulos, F., “Evaluation of bio-prosthetic heart valve performance in patient-specific configuration: a feasibility study from MRI data,” Biomedical Engineering Society: 2010 Meeting, Austin, TX, October 2010.

35. Le, T., Borazjani, I., Sotiropoulos, F., “Simulation of a bi-leaflet mechanical heart valve (BMHV) in a left heart system,” The 6th World Congress on Biomechanics, Singapore, August 2010.

36. Wu, J., Yun, B. M., Fallon, A. M., Simon, H. A., Aidun, C. K., Yoganathan, A. P., “Numerical investigation of blood damage in the hinge area of bileaflet mechanical heart valves,” American Society of Mechanical Engineers: Summer Bioengineering Conference, Naples, FL, June 2010.

37. Le, T., Borazjani, I., Sotiropoulos, F., “Fluid Structure Interaction simulation of heart prosthesis in patient-specific left-ventricle/aorta anatomies,” 62nd Annual Meeting of APS Division of Fluid Dynamics, Minneapolis, MN, November 2009.

38. Yap, C. H., Dasi, L. P., Yoganathan, A. P., “Dynamic Energy Loss Characteristics in the Native Aortic Valve,” 62nd Annual Meeting of APS Division of Fluid Dynamics, Minneapolis, MN, November 2009.

39. Dasi, L. P., Ge, L., Borazjani, I., Simon, H. A., Sotiropoulos, F., Yoganathan, A. P. “Experimental Requirements For Validating High Resolution FSI-CFD Tools For Heart Valve Modeling,” FDA/NHLBI /NSF Workshop on Computer Methods for Cardiovascular Devices, Rockville, Maryland, June 2009.

40. Yap, C. H., Kim, H. S., Dasi, L. P., Weiler, M., Balachandran, K., Haj-Ali, R., Yoganathan, A. P., “Structural Deformation of Native Aortic Valve Leaflet Under Hypertension: An In Vitro Study,” ASME Summer Bioengineering Conference, Lake Tahoe, CA, June 2009.

41. Simon, H. A., Ge, L., Dasi, L. P., Borazjani, I., Leo, H. L., Sotiropoulos, F., Yoganathan, A. P., “Numerical Simulations of The Three-Dimensional Pulsatile Hinge Flow Fields of Bileaflet Mechanical Heart Valves,” FDA/NHLBI /NSF Workshop on Computer Methods for Cardiovascular Devices, Rockville, MD, June 2009.

42. Borazjani, I., Le, T., Sotiropoulos, F., “A multi-block/immersed boundary numerical framework for simulating cardiovascular flows,” FDA/NHLBI /NSF Workshop on Computer Methods for Cardiovascular Devices, Rockville, MD, June 2009.

43. Simon, H. A., Ge, L., Sotiropoulos, F., Yoganathan, A. P., “Numerical Study of the Influence of the Hinge Gap Width on The Hinge Flow Fields of Bileaflet Mechanical Heart Valves”, 61st Annual meeting of APS Division of Fluid Dynamics, San Antonio, TX, November 2008.

44. Yap, C. H., Dasi, L. P., Rusly, R. J., Yoganathan, A. P., “Dynamics of the Aortic Valve Under Normal, Flow Rate-Varied and Heart Rate-Varied Conditions: An In Vitro Study”, ASME Summer Bioengineering Conference, Marco Island, FL, June 2008.

45. Simon, H.A., Ge, L., Borazjani, I., Sotiropoulos, F., and Yoganathan, A.P. ,“Simulations Of The Hinge Flow Fields Of A Bileaflet Mechanical Heart Valve Under Physiologic Pulsatile Aortic Conditions”, ASME Summer Bioengineering Conference, Marco Island, FL, June 2008.

46. Murphy, D.W., Dasi, L.P., Glezer, A., and Yoganathan, A.P., “Reduction of Flow-Induced Blood Damage In Bileaflet Mechanical Heart Valves Through Passive Flow Control”, ASME Summer Bioengineering Conference, Marco Island, FL, June, 2008.

47. Simon, H., Dasi, L.P., Leo, H.W., Fallon, A., and Yoganathan, A.P., “Fluid Mechanics of Prosthetic Heart Valves”, Inaugural International Conference of the Engineering Mechanics Institute (EM08), Minneapolis, MN, May 18-21, 2008.

48. Le, T., Borazjani, I., Sotiropoulos, F., “The 3D vorticity dynamics of impulsive flow through an inclined nozzle,” 61st Annual meeting of APS Division of Fluid Dynamics, San Antonio, TX, November 2008.

49. Dasi, L.P., Murphy, D.W., Glezer, A., and Yoganathan, A.P., “Reduction of the Pro-Coagulant Potential of Bileaflet Mechanical Heart Valves using Passive, Surface-Mounted Elements”, Fifth International Bio-Fluid Symposium and Workshop, California Institute of Technology, Pasadena, CA, March 28 - 30, 2008.

IN PREPARATION

1. Yun, B.M., Aidun, C.K., and Yoganathan, A.P. “Simulations of Pulsatile Suspension Flow through a Bileaflet Mechanical Heart Valve” (in preparation)

2. Yun, B.M., McElhinney, D., Aidun, C.K., and Yoganathan, A.P. “Predictive Modeling of Suspension Flow through Bileaflet Mechanical Heart Valves with Pediatric Conditions” (in preparation)

3. Jun, B.H., Yoganathan, A.P., Arjunon, S., Saikrishnan, N. “In Vitro Micro Particle Image Velocimetry investigation of the effect of hinge gap width on a bileaflet mechanical heart valve” (in preparation)

4. Santhanakrishnan, A., Okafor, I., Angirish, Y., Yoganathan, A. P., “E□ect of varying heart rate on intra-ventricular filling fluid dynamics”

5. Okafor, I., Angirish, Y., Yoganathan, A. P., Santhanakrishnan, A., “E□ect of mitral orifice shape on intra-ventricular filling fluid dynamics” (in preparation)

6. Santhanakrishnan, A., Okafor, I., Chaffins, B., Yoganathan, A. P., "Vortex dynamics of inclined nozzle in confined domain" (in preparation)

7. Le, T. B., Sotiropoulos, F., Mirabella, L., Okafor, I., Santhanakrishnan, A., Oshinski, J. N., Yoganathan, A. P., "Validation of numerical simulation of Left Ventricular Hemodynamics Guided by *in-vivo* Cardiac Magnetic Resonance Data: diastolic filling" (in preparation)

8. Le, T. B., Sotiropoulos, F., Mirabella, L., Okafor, I., Santhanakrishnan, A., Oshinski, J. N., Yoganathan, A. P., "Validation of numerical simulation of Left Ventricular Hemodynamics Guided by *in-vivo* Cardiac Magnetic Resonance Data: systolic ejection" (in preparation)